ELEMENTA
Science of the Anthropocene

Huang, Y, et al. 2022. Toward a more realistic representation of surface albedo in NASA CERES-derived surface radiative fluxes: A comparison with the MOSAiC field campaign. *Elem Sci Anth*, 10: 1. DOI: https://doi.org/10.1525/elementa.2022.00013

RESEARCH ARTICLE

Toward a more realistic representation of surface albedo in NASA CERES-derived surface radiative fluxes: A comparison with the MOSAiC field campaign

Yiyi Huang[1], Patrick C. Taylor[2,*], Fred G. Rose[1], David A. Rutan[1], Matthew D. Shupe[3,4], Melinda A. Webster[5], and Madison M. Smith[6]

Accurate multidecadal radiative flux records are vital to understand Arctic amplification and constrain climate model uncertainties. Uncertainty in the NASA Clouds and the Earth's Radiant Energy System (CERES)-derived irradiances is larger over sea ice than any other surface type and comes from several sources. The year-long Multidisciplinary drifting Observatory for the Study of Arctic Climate (MOSAiC) expedition in the central Arctic provides a rare opportunity to explore uncertainty in CERES-derived radiative fluxes. First, a systematic and statistically robust assessment of surface shortwave and longwave fluxes was conducted using in situ measurements from MOSAiC flux stations. The CERES Synoptic 1degree (SYN1deg) product overestimates the downwelling shortwave flux by +11.40 Wm^{-2} and underestimates the upwelling shortwave flux by –15.70 Wm^{-2} and downwelling longwave fluxes by –12.58 Wm^{-2} at the surface during summer. In addition, large differences are found in the upwelling longwave flux when the surface approaches the melting point (approximately 0°C). The biases in downwelling shortwave and longwave fluxes suggest that the atmosphere represented in CERES is too optically thin. The large negative bias in upwelling shortwave flux can be attributed in large part to lower surface albedo (–0.15) in satellite footprint relative to surface sensors. Additionally, the results show that the spectral surface albedo used in SYN1deg overestimates albedo in visible and mid-infrared bands. A series of radiative transfer model perturbation experiments are performed to quantify the factors contributing to the differences. The CERES-MOSAiC broadband albedo differences (approximately 20 Wm^{-2}) explain a larger portion of the upwelling shortwave flux difference than the spectral albedo shape differences (approximately 3 Wm^{-2}). In addition, the differences between perturbation experiments using hourly and monthly MOSAiC surface albedo suggest that approximately 25% of the sea ice surface albedo variability is explained by factors not correlated with daily sea ice concentration variability. Biases in net shortwave and longwave flux can be reduced to less than half by adjusting both albedo and cloud inputs toward observed values. The results indicate that improvements in the surface albedo and cloud data would substantially reduce the uncertainty in the Arctic surface radiation budget derived from CERES data products.

Keywords: Arctic surface energy budget, Sea ice surface albedo, Satellite-derived surface energy budget

1. Introduction

Warming in the Arctic has increased more than twice as fast as the rest of the world over the past 4 decades, a phenomenon called Arctic amplification (Holland and Bitz, 2003). The rapid and unprecedented changes in the Arctic alter the region's surface climate with significant implications for the surface energy budget (e.g., Lee et al., 2017). The underlying mechanisms of these rapid Arctic changes remain unclear (e.g., Taylor et al., 2021). Therefore, accurate multidecadal radiative flux records are vital to understand Arctic amplification and constrain climate model spread or uncertainties (Lesins et al., 2012; Baker and Taylor, 2016; Duncan et al., 2020).

[1] Science Systems and Applications, Inc., Hampton, VA, USA
[2] NASA Langley Research Center, Hampton, VA, USA
[3] Cooperative Institute for Research in Environmental Sciences, University of Colorado Boulder, Boulder, CO, USA
[4] Physical Sciences Laboratory, National Oceanic and Atmospheric Administration, Boulder, CO, USA
[5] Geophysical Institute, University of Alaska Fairbanks, Fairbanks, AK, USA
[6] Applied Physics Laboratory, University of Washington, Seattle, WA, USA

* Corresponding author:
Email: patrick.c.taylor@nasa.gov

Observing the Arctic from space is one of the most challenging tasks in climate science. The Arctic surface energy budget is difficult to measure and poorly understood because of its unique environment, including the high albedo of the snow/ice surface, substantial spatial and temporal heterogeneity in surface properties (e.g., optics, thermal conductivity, surface roughness, leads/ponds), large solar zenith angle, the absence of solar radiation during winter, extremely low temperature and humidity, the presence of temperature inversions, and the frequent occurrence of supercooled mixed-phase clouds (Curry, 1996; Shupe and Intrieri, 2004; Walsh, 2009; Duncan et al., 2020). The Clouds and the Earth's Radiant Energy System (CERES) provides satellite retrieved surface irradiances at various temporal and spatial scales (Kato et al., 2018) that are widely used in analyses of regional and global mean surface irradiances (e.g., Hakuba et al., 2016), for constraining other energy fluxes (e.g., DeAngelis et al., 2015; Boos and Korty, 2016), as well as for evaluating climate models (e.g., Boeke and Taylor, 2016). However, uncertainty in CERES irradiances is substantially larger over sea ice than any other surface type (Su et al., 2015). For instance, Huang et al. (2017b) compared the CERES Energy Balanced and Filled (EBAF) derived monthly radiative fluxes with 5 Baseline Surface Radiation Network stations over the Arctic finding biases (root-mean-square error [RMSE]) of $+2.27$ (4.91) Wm^{-2} and $+4.41$ (6.17) Wm^{-2} for downwelling shortwave (SW down) and longwave (LW down) fluxes, respectively. Riihela et al. (2017) compared CERES SYN1deg data against in situ observations from the Tara drifting station, finding that over sea ice the upwelling shortwave (SW up) flux at the surface is too low due to a large negative bias in sea ice albedo, while the upwelling longwave (LW up) flux over sea ice saturates during mid-summer. Comparisons with airborne in situ measurements also suggest that CERES Synoptic 1degree (SYN1deg) SW up flux is too low (Smith et al., 2017). More recently, Kato et al. (2018) estimated uncertainty values for the Arctic surface radiative flux terms ranging from 12 to 16 (1σ) Wm^{-2} at the monthly $1^\circ \times 1^\circ$gridded scale, with the regional annual mean bias ranging from -4 to 4 Wm^{-2}.

These uncertainties in surface radiative fluxes come from a variety of sources. Uncertainty in atmospheric temperature and humidity from reanalysis, heterogeneity in surface conditions (including sea ice properties, snow cover, and albedo; Su et al., 2015), and difficulties detecting and characterizing clouds over sea ice all contribute to the CERES irradiance uncertainty (Kato et al., 2018). Moreover, clouds are gridded to, and radiative transfer calculations are done on, a quasi-equal area grid in the polar regions, which could hinder the ability to represent fluxes in the central Arctic (Riihela et al., 2017). In addition to atmospheric and cloud input, errors associated with the radiative transfer model (RTM) add another layer of uncertainty to surface radiation retrievals, such as assumption of a gamma distribution of cloud optical thickness and treatment of vertical correlation of cloud properties (Kato et al., 2005). Understanding these multiple potential sources of uncertainty in CERES-derived surface radiative fluxes in the central Arctic requires a thorough exploration of in situ observations of the thermodynamic and radiative properties of the atmosphere and surface.

Direct, in situ time series over the central Arctic are rare. To address needs for cross-disciplinary, process-level understanding of the changing Arctic and thereby advance satellite observations and models, an international consortium of scientists and institutions conducted the most comprehensive exploration of the central Arctic system in history. Starting in October 2019, the German icebreaker *Polarstern* left Norway, as a part of the Multidisciplinary drifting Observatory for the Study of Arctic Climate (MOSAiC) expedition, traveled through the northern Laptev Sea and moored itself inside the freezing sea ice pack. Over the next 10 months, the *Polarstern* passively drifted with the sea ice across the central Arctic, until reaching the ice edge in the Fram Strait on July 31, 2020, about 1,800 km from its starting position. After July 2020, the *Polarstern* relocated further north to continue measurements from late August to late September 2020. The MOSAiC ship track during April–September 2020 is shown in **Figure 1**. The MOSAiC expedition provides a comprehensive set of observations of the Arctic climate system, to link the atmosphere, sea ice, and ocean through physical, chemical, and biological pathways (Shupe et al., 2020). Therefore, the MOSAiC field campaign provides an incredible opportunity to quantify and reduce uncertainty in CERES radiative fluxes over sea ice in the central Arctic.

In this study, a systematic and statistically robust assessment of surface shortwave and longwave radiative fluxes is performed using in situ measurements from MOSAiC, including measurements from multiple locations on the sea ice within approximately 15 km of the drifting *Polarstern*. We focus on surface radiative fluxes during the 2020 melt season (April–September), noting that the sea ice changes rapidly during the melt season and thereby exerts a large influence on the surface radiation budget (Persson, 2012; Huang et al., 2017a; Huang et al., 2019). CERES satellite observations and retrievals over the Arctic are more reliable in summer than in winter (Huang et al., 2017b). We are particularly interested in shortwave albedo changes that are only relevant during the summer. Further, a series of perturbation experiments with the Langley Fu–Liou RTM (Fu and Liou, 1993; Fu et al., 1998) are performed, by utilizing the surface conditions measured during the MOSAiC field campaign to quantify contributions to the flux differences. In this study, we focus on surface albedo because it is thought to be one of the most uncertain input sources in CERES products (e.g., Riihela et al., 2017; Kato et al., 2018; Diagio et al., 2021) and is expected to be the largest contributor toward the large shortwave flux uncertainty. The goal of this study is to understand the sources of uncertainty in the Arctic surface radiation budget derived from CERES to reduce these uncertainties and benefit the Arctic climate science community.

2. Data and methodology

2.1. MOSAiC surface measurements and retrievals

We use radiation and meteorological measurements from 3 stations at MOSAiC (Shupe et al., 2021; flux station

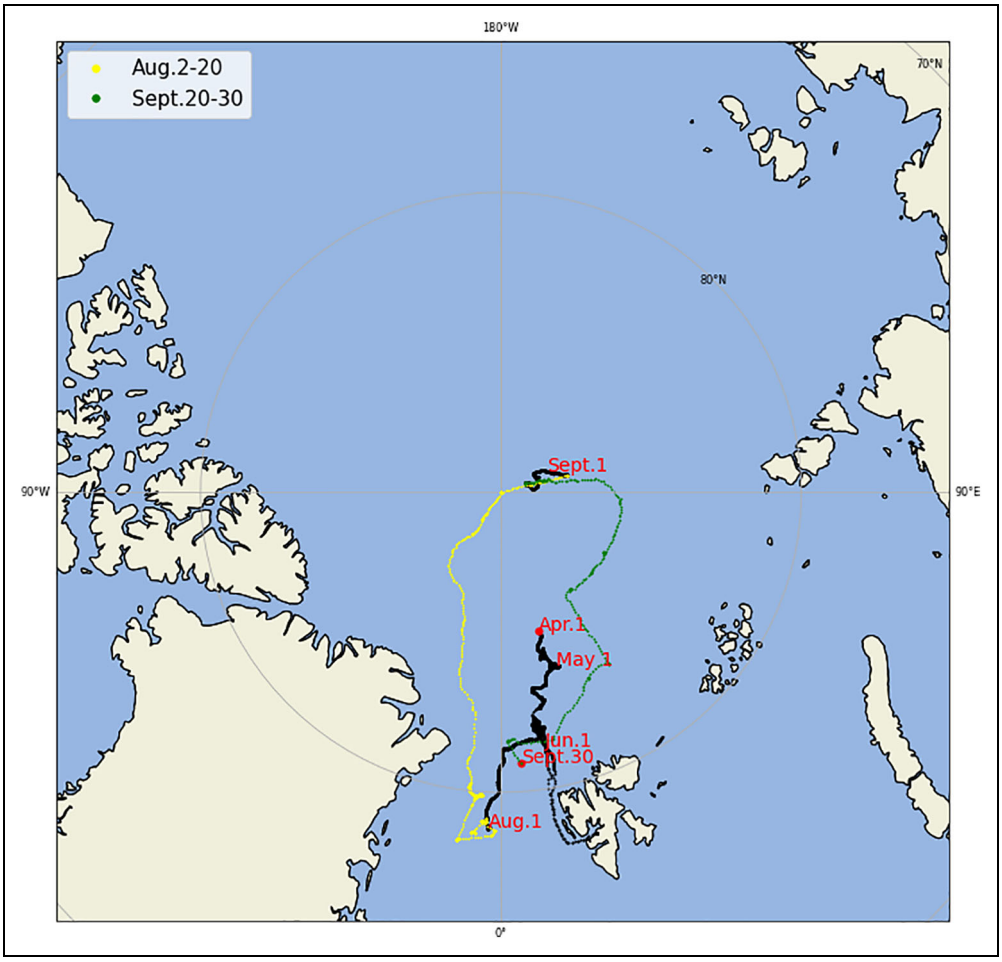

Figure 1. The research vessel *Polarstern* ship track during April–September 2020, as a part of the MOSAiC expedition. The flux station measurements during August 2–20 (yellow) and September 20–30 (green) are removed from analysis because the measurements were made from onboard the ship in transit. DOI: https://doi.org/10.1525/elementa.2022.00013.f1

measurements, hereafter). The flux stations included a variety of measurements including a full suite of upward and downward looking broadband radiometers operated by the U.S. Department of Energy Atmospheric Radiation Measurement Program. The upwelling and downwelling solar radiative fluxes were measured by a pair of Eppley Precision Solar Pyranometers (295–3,000 nm), while the upwelling and downwelling terrestrial radiative fluxes were measured by a pair of Eppley Precision Infrared Radiometers (3,500–50,000 nm). The downward viewing radiometers were positioned at a nominal height of 3 m above the surface. Similar broadband solar and terrestrial radiative fluxes were measured by the University of Colorado/National Oceanic and Atmospheric Administration (NOAA) surface flux team at 2 Atmospheric Surface Flux Stations (ASFS30 and 50) installed at variable distances up to about 10 km away from Met City (Cox et al., 2021a; Cox et al., 2021b; Cox et al., 2021c). The upwelling and downwelling solar and terrestrial radiative fluxes were measured by pairs of Hukseflux SR30 pyranometers (285–3,000 nm) and IR20 pyrgeometers (10,000–40,000 nm) mounted at a nominal height of 2 m above the surface. Based on the heights of the downward looking radiometers at the different sites, the measurements are representative of a circular area of about 6–14 m^2 underneath the radiometers, which was typically dominated by sea ice with only marginal influences from nearby melt ponds. Additional measurements of the near-surface meteorology and turbulent heat fluxes were made at 2, 6, and 10 m at Met City and at 2–3 m at the ASFSs. Note that instrument calibration adjustments and a variety of quality control processes have been applied to these data sets. While the raw measurements were made at higher temporal resolution, we use 10-min ASFS and Met City data to evaluate CERES hourly surface radiative fluxes. Note that there are data quality issues and/or the data were not obtained for scientific uses during certain periods at different sites. Particularly, during August 2–20 and September 20–30, 2020, all flux station measurements are removed from the analysis (**Figure 1**).

From June to September 2020, surface spectral albedo measurements were carried out along multiple survey lines (survey line measurements hereafter), ranging in length from 60 m to 200 m. The measurement spacing was 5 m, and the survey lines were visited 1–6 times per week. Measurements were made using an analytical spectral devices spectroradiometer (Grenfell and Perovich, 2008) with a spectral range of 350–2,500 nm and

reported integrated values every 1 nm based on observations made every 1.4–2 nm. The survey lines were placed on sea ice deemed representative of sea ice conditions in the broader area and included a mixture of snow, bare sea ice, melt ponds, and sediment-laden ice. For more details on the data processing and quality control, see Smith et al. (2021a; 2021b) and Light et al. (2021). It should be noted that there are 18 shortwave spectral bands (175.4–4,000 nm) used by CERES (Rutan et al., 2015). Therefore, the spectral albedo from MOSAiC has been averaged for each CERES band within the overlapping spectral range (357.5–2,500 nm), resulting in 10 bands for comparison between 2 data sets.

To evaluate CERES products, we use surface spectral albedo from the MOSAiC survey line measurements, while surface broadband albedo, radiative fluxes and meteorological observations are obtained from the MOSAiC flux station measurements. Note that the broadband albedo measurements are also available from MOSAiC survey line (Light et al., 2021). Here, we compare the broadband albedo from survey line and flux station measurements on daily scale (Figure S1). They are in a good agreement in general, with the mean value being slightly higher in flux station than that of survey line by 0.05 (7.50%). It is probably because the flux station is dominated by sea ice, while the survey line included a mixture of snow, bare sea ice, melt ponds, and sediment-laden ice. Note that different spectral ranges (flux station: 285–3,000 nm, survey line: 300–3,000 nm) and temporal coverage between survey line and flux station may contribute to the broadband albedo difference. Since the goal of study is to evaluate how surface albedo bias impacts on surface radiative flux retrievals, we use broadband albedo from flux station measurements to evaluate CERES products.

2.2. CERES satellite observations and retrievals

The CERES data sets used in this study include CERES Synoptic (SYN1deg-Month and SYN1deg-Hour) and EBAF Edition 4.1 (Ed4.1) products. The CERES SYN1deg product provides high-quality global hourly and monthly $1^\circ \times 1^\circ$ gridded top-of-atmosphere (TOA), in-atmosphere, and surface radiative fluxes. The in-atmosphere and surface fluxes are computed hourly using the Langley-modified Fu–Liou RTM based upon inputs from *Terra* and *Aqua* Moderate Resolution Imaging Spectroradiometer (MODIS), 3-hourly geostationary (GEO) data, and meteorological assimilation data from the Goddard Earth Observing System Version 5.4.1 (GEOS-5.4.1; Rutan et al., 2015).

In addition to SYN1deg, the CERES EBAF Ed4.1 data set, with a monthly temporal scale and $1^\circ \times 1^\circ$ spatial resolution, is compared with MOSAiC surface measurements. The Ed4.1 EBAF-Surface algorithm adjusts SYN1deg-Month surface irradiances by 2 processes: bias correction and Lagrange multiplier. Biases in surface irradiances caused by biases in temperature, humidity, and cloud fraction with known sign are adjusted in the bias correction process. To minimize the difference between computed and observed TOA longwave and shortwave irradiances, the Lagrange multiplier technique is used to adjust surface, atmospheric, and cloud properties by region after the bias correction (Kato et al., 2018). Note that only all-sky surface radiative fluxes from SYN1deg and EBAF products are compared with MOSAiC observations.

To collocate MOSAiC surface observations and CERES hourly data products, the 10-min MOSAiC files are first averaged by hour, and then each hour is matched with the nearest $1^\circ \times 1^\circ$ grid box in SYN1deg-Hour and EBAF products. The point-by-point MOSAiC and SYN1deg-Hour comparison results below only include days when there are at least 2 measurements available among ASFS30, ASFS50, and Met City; this is performed to mitigate differences due to the comparison of point measurements with the CERES $1^\circ \times 1^\circ$ grid box. The MOSAiC observation is obtained by averaging all available measurements.

In addition, since the MOSAiC measurement is compared with SYN1deg data at the $1^\circ \times 1^\circ$ grid scale, it is necessary to explore spatial inhomogeneity influences on the SYN1deg-Hour bias. Specifically, spatial heterogeneity is defined as the ratio (in percentage) between the "absolute variance" and the average of all available MOSAiC measurements. The absolute variance is the maximum difference among each pair of measurements (ASFS30 and ASFS50, ASFS30 and Met City, ASFS50 and Met City) at a given time.

2.3. Langley modified Fu—Liou RTM and CERES SYN1deg flux computation

To determine which input data contributes to the uncertainties in SYN1deg product, the first step is to run a CERES-like calculation to reproduce the surface radiative fluxes through the RTM during the MOSAiC observing period (control run hereafter), which is described in this section. In comparison, Section 2.4 describes how we perturb surface albedo and cloud properties to examine the sensitivity of surface radiative fluxes to those changes (perturbation run hereafter).

As mentioned earlier, the in-atmosphere and surface radiative fluxes in SYN1deg are computed hourly in approximate equal-area grid boxes using the Langley Fu–Liou RTM (Fu and Liou, 1993; Fu et al., 1998; Kratz and Rose, 1999; Kato et al., 1999; Kato et al., 2005). A list of the longwave and shortwave bands in the current model is given in Rutan et al. (2015) and Rose et al. (2006). Note that the band structure used in computations is modified from the original Fu–Liou code and different from Kato et al. (1999). Gaseous absorption in the shortwave region is treated by the method described in Kato et al. (1999) and accounts for absorption by water vapor, carbon dioxide, ozone, methane, and oxygen. For carbon dioxide, methane, and nitrous oxide, secularly increasing values are used from the NOAA Global Monitoring Laboratory's annual greenhouse gas index (AGGI; https://gml.noaa.gov/aggi/aggi.html). Gaseous longwave absorption is treated by the method described in Kratz and Rose (1999). A complete description of the RTM can be found in Rose et al. (2013).

The RTM calculations require numerous input data sets including meteorological conditions, cloud and aerosol properties, ozone profiles, surface spectral and broadband albedo, snow and ice conditions, and so on. A detailed

Table 1. The input sources for Fu–Liou radiative transfer model in this study. DOI: https://doi.org/10.1525/elementa.2022.00013.t1

Category	Variables	Sources
General model inputs	Number of model cloud layers	Four layers
	Solar zenith angle	MODIS
	Solar insolation	Daily Solar Radiation and Climate Experiment and Total Solar Irradiance files and earth–sun distance
	Solver method	Four-stream solver for shortwave and longwave calculations
	CO_2, CH_4, N_2O, CFCs concentrations	NOAA Earth System Research Laboratories annual greenhouse gas index
Atmospheric structure inputs	Pressure profile	GEOS-5.4.1 reanalysis
	Air temperature profile	
	Water vapor mixing ratio profile	
	Ozone mixing ratio profile	
	Surface skin temperature	
Cloud inputs	Cloud fraction, effective radius, optical depth, phase, particle size	MODIS
Surface inputs	Spectral surface albedo	JIN lookup table, daily sea ice concentration, and monthly Terra surface albedo history map
	Spectral surface emissivity	Determined by surface type
Aerosol inputs	Aerosol types and aerosol optical depth	MATCH aerosol hourly output

MODIS = Moderate Resolution Imaging Spectroradiometer; NOAA = National Oceanic and Atmospheric Administration.

description of model inputs for SYN1deg product is given in Rutan et al. (2015). **Table 1** provides a list of ancillary inputs used to calculate surface radiative fluxes in this study. In addition to general model inputs and atmospheric structure profiles, ozone profiles come from the National Centers for Environmental Prediction Stratosphere Monitoring Ozone Blended Analysis product (Yang et al., 1998). Cloud properties, including fraction, effective radius, optical depth, phase, and particle size, are derived from MODIS and multiple GEO satellites imagers. At high latitudes, however, no GEO data are used, but sampling by *Terra* and *Aqua* increases. Given that a bias was found when validating retrievals over the Antarctic after initial code development, the CERES team applied a correction to cloud optical depth for polar daytime retrievals in SYN1deg Ed4 product. We adopted this methodology to make sure our RTM calculations are consistent with CERES SYN1deg production process. Specifically, the natural log of cloud optical depth is reduced by one during the polar daytime (solar zenith angle > 0) when sea ice concentration is greater than 99%.

Surface albedo information comes from multiple sources. The ocean and sea ice spectral albedos are estimated by a lookup table (LUT) based on the Coupled Ocean–Atmosphere Radiative Transfer model described by Jin et al. (2004). A surface albedo history (SAH) map provides monthly broadband surface albedo information for each CERES grid box, derived from observed TOA albedo from *Terra* and *Aqua* satellites, meteorology, and surface type. The initial spectral albedo is normalized to broadband albedo such that the integral of the spectral albedo equals the broadband surface albedo. Snow and ice information comes from National Snow and Ice Data Center daily maps supplemented by maps from NOAA NESDIS and a cryosphere flag derived from the MODIS clear-sky imager. Emissivity over land and water is derived in 12 spectral bands based on surface scene type (Wilber et al., 1999) as defined by the International Geosphere-Biosphere Programme map of 17 Earth surface types along with fresh snow and ice (Rutan et al., 2009).

Aerosol information comes from satellite-derived sources as well as from a global chemical assimilation model (Remer et al., 2005). In this case, aerosol optical depth (AOD) comes from the Model for Atmospheric Transport and Chemistry (MATCH; Collinset al., 2001). MATCH is a global chemical transport model that assimilates MODIS retrievals of AOD using Collection 5 after May 2006. MATCH defines aerosol constituents throughout the vertical atmospheric column using Optical Properties of Aerosols and Clouds from Hess et al. (1998) and desert dust from Tegen and Lacis (1996).

Note that most inputs and data-processing procedures for the RTM calculations in this study are identical to the CERES SYN1deg production process, except for the solver method. To generate the SYN1deg product, a gamma-weighted two stream approximation (GWTSA) model (Kato et al., 2001; 2005) is used to compute the shortwave flux vertical profile for each cloud layer. A modified

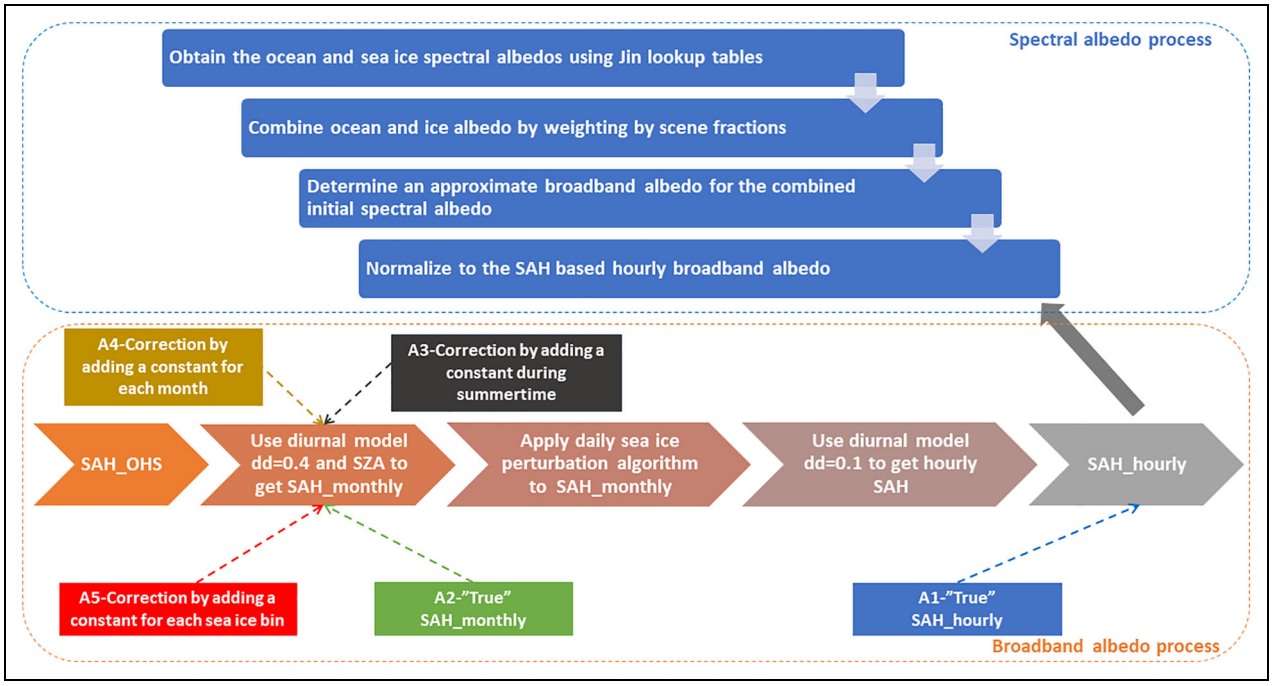

Figure 2. The surface albedo perturbation experimental design using Fu–Liou radiative transfer model. DOI: https://doi.org/10.1525/elementa.2022.00013.f2

2-stream approximation (Toon et al., 1989; Fu et al., 1998) has been used for longwave flux computation. In this study, we use the Langley Fu–Liou four-stream solver (Kato et al., 2005) for both longwave and shortwave flux calculations. This choice is made because the GWTSA solution reaches a numerical singularity under conditions with a highly reflective surface and in the presence of an optically thick low cloud in the band near 400 nm when single scatter albedos are close to 1.0, generating unrealistic fluxes. In addition, the GWTSA does not perform well when geometrically thick clouds are distributed in multiple model vertical layers. We ran RTM simulations for May and June to estimate the influence of the GWTSA versus the four-stream solver and showed no differences in the longwave fluxes, a 3% (approximately 7 Wm^{-2}) difference in SW down, and a 2% (approximately 3 Wm^{-2}) difference in SW up. In both cases, the four-stream solver provided a better agreement with MOSAIC in situ observations. The choice of solver does not change our conclusions. As for the monthly broadband albedo source, we tested both *Terra* and *Aqua* SAH in SYN1deg Ed4 and found no substantial differences in the results; thus, we use *Terra* SAH only to simplify the calculations.

Figure 2 illustrates all steps in the SYN1deg production process (Rutan et al., 2015) to produce the surface albedo in the RTM and provides a diagram of the surface albedo perturbation experimental design. First, at each $1^\circ \times 1^\circ$ grid box, the ocean and sea ice spectral albedos are obtained using the LUTs described in Jin et al. (2004). The initial combined spectral albedo is obtained by a weighted average of sea ice and ocean scene fractions. The broadband albedo is determined using the combined spectral albedo and then is adjusted based on SAH hourly broadband albedo (SAH_hourly).

As mentioned earlier, the SAH map provides monthly broadband surface albedo information at overhead sun (SAH_OHS) for each CERES grid box. Therefore, there are several steps to convert monthly SAH_OHS to SAH_hourly. First, using the solar zenith angle at each hour, we apply a diurnal model to compute SAH monthly, diurnal monthly average broadband albedo (SAH_monthly). The diurnal model is described by Briegleb et al. (1986) and Rutan et al (2015). Next, the SAH_monthly is adjusted using the sea ice anomaly difference between the daily and monthly mean sea ice concentrations. The diurnal model is applied again with a different coefficient to get SAH hourly broadband albedo (SAH_hourly) from the monthly, diurnal average. The SAH_hourly value is used to normalize the initial broadband albedo in the RTM.

2.4. RTM calculation and perturbation experiments

The control run, described in Section 2.3, uses the inputs described in **Table 1**, which is consistent with the SYN1-deg production process. To further understand the radiative impact of surface albedo differences between CERES and MOSAiC, we perform 5 broadband albedo perturbation experiments, adjusting the SAH in different ways. A detailed description of each surface albedo experiment is provided in **Table 2**. The first albedo perturbation experiment (A1) replaces SAH_hourly with hourly surface albedo measured by MOSAiC ASFS30, while the second experiment (A2) replaces the SAH_monthly with the one averaged from MOSAiC flux station observations for each month. In the third (A3) and fourth (A4) experiments, we correct SAH_monthly by adding a constant for the entire summer (+0.15) and then for each month (+0.10−0.22), respectively. Corrections are derived from the comparison between collocated SYN1deg-Hour data and MOSAiC measurements (Section 3). In addition, we correct SAH_monthly by adding a sea ice concentration dependent correction factor in the fifth experiment (A5). Note

Table 2. The description of surface albedo perturbation experimental design. DOI: https://doi.org/10.1525/elementa.2022.00013.t2

Category	Experiment	Description
Broadband albedo perturbation experiments	Control run	Default TERRA monthly Surface Albedo History map
	A1—"True" SAH_hourly	Replace SAH_hourly with MOSAiC hourly albedo
	A2— "True" SAH_monthly	Replace SAH_monthly with MOSAiC monthly albedo
	A3—Correction to SAH_monthly by a constant in summer	Correct bias in SAH_monthly by adding 0.15 during summer
	A4—Correction to SAH_monthly by a constant for each month	Correct bias in SAH_monthly by adding a different constant for each month
	A5—Correction to SAH_monthly by weighted surface albedo for each sea ice bin	Correct bias in SAH_monthly by adding a different constant for each sea ice bin; the constant is weighted by sea ice fraction at corresponding time step
Spectral albedo perturbation experiments	A6—Monthly averaged spectral albedo from control run (June–September)	Replace initial spectral albedo with monthly averaged spectral albedo obtained from control run from June to September
	A7—Monthly averaged spectral albedo from MOSAiC (June–September)	Replace initial spectral albedo with monthly averaged spectral albedo measured by MOSAiC from June to September

MOSAiC = Multidisciplinary drifting Observatory for the Study of Arctic Climate.

that the correction factor was weighted by the sea ice concentration at a given location such that the adjustments are only applied to the sea ice portions of the grid box, which is shown in Equation 1.

$$\text{Corrected SAH}_{\text{monthly}} = \text{Initial SAH}_{\text{monthly}} + \text{Alb\_bias}_k * \text{SIC}, \quad (1)$$

where Alb bias_k represents the albedo bias in SYN1deg-Hour product relative to MOSAiC for each sea ice bin (**Figure 3**) and k indicates the *k*th sea ice bin, ranging from 1 to 10. In this experiment, we only apply an albedo correction to the sea ice portion of CERES 1°×1° grid box because measured irradiances represent the sea ice type.

In addition to the broadband albedo perturbation, we run 2 additional experiments, A6 and A7, replacing the initial spectral albedo with the monthly averaged spectral albedo obtained from a CERES-like RTM control run and the MOSAiC spectral albedo from June to September, respectively. The monthly averaged spectral albedo inputs used in the RTM are shown in Figure S4. Note that MOSAiC spectral albedos are not available within bands 0.1754–0.2247 μm and 2.50–4.00 μm to be matched with CERES spectral ranges. Therefore, we extrapolate the missing values in those bands by multiplying the corresponding albedo in the CERES-like RTM by the ratio between RTM albedo and MOSAiC albedo in the nearest band.

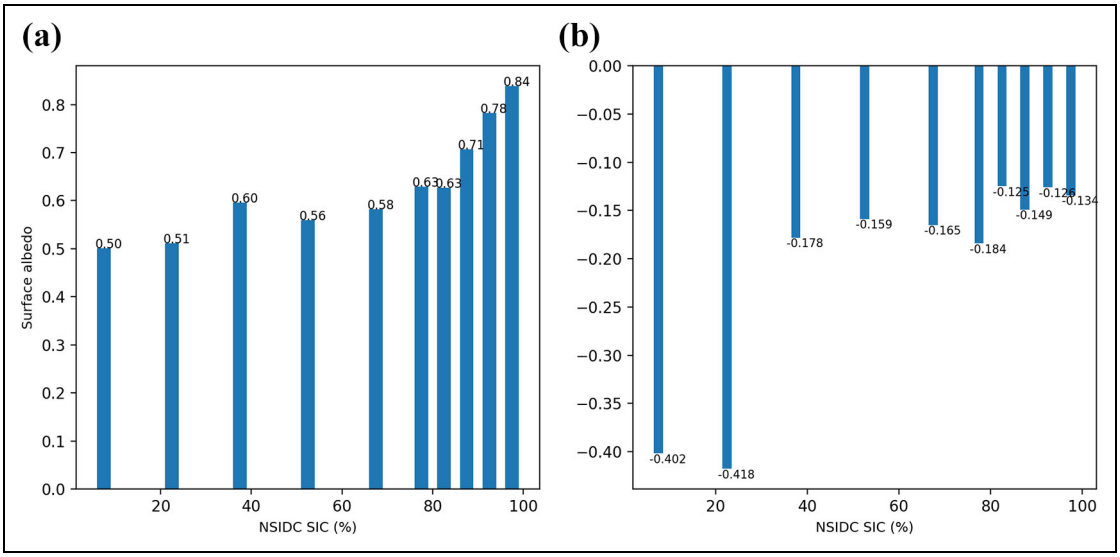

Figure 3. The bin-averaged (a) surface albedo measured by MOSAiC ASFS30 remote flux station and (b) CERES SYN1deg surface albedo bias in CERES SYN1deg relative to the MOSAiC measurements as a function of sea ice concentration. DOI: https://doi.org/10.1525/elementa.2022.00013.f3

Table 3. The description of cloud perturbation experimental design. DOI: https://doi.org/10.1525/elementa.2022.00013.t3

Experiment	Description
C1—Increase cloud fraction by 1%	Increase total cloud fraction by 1% (increase cloud fraction by 1%/n at each cloud layer, while *N* represents the number of cloud layer)
C2—Increase cloud fraction by 3%	Increase total cloud fraction by 3% (increase cloud fraction by 1%/n at each cloud layer, while *N* represents the number of cloud layer)
C3—Uncorrected retrieved cloud optical depth is being used	Uncorrected retrieved cloud optical depth is being used, which means increase natural log of cloud optical depth by 1 when sea ice >99% during polar daytime
C4—Combine C1 and C3	Increase both cloud fraction and cloud optical depth as described in C1 and C3
C5—Combine C2 and C3	Increase both cloud fraction and cloud optical depth as described in C1 and C3

Note that all cloud experiments were performed with surface albedo correction as described in Experiment A5, which means that the SAH_monthly was corrected by adding a constant for each sea ice bin.

Biases in cloud properties are also an important factor that contributes to uncertainties in derived surface radiative fluxes. The results of the surface albedo experiments below (Section 4) revealed that the SW up improved markedly between CERES and MOSAiC with improved surface albedo information; however, the differences in the SW down increased. This increase in the SW down flux (described in Section 4) results from the reflection of the increased SW up flux back toward the surface by clouds. Therefore, on top of surface albedo experiment A5, we perform a series of cloud perturbation experiments to better understand how the results change after adjusting cloud properties within uncertainty bounds.

The description of the experimental design is given in **Table 3**. In the first (C1) and second (C2) experiments, we increase the total cloud fraction by 1% and 3%, respectively. Specifically, the cloud fraction has been increased by 1% (or 3%)/N at each cloud layer, where N represents the number of cloud layers. Yost et al. (2020) compared the CERES MODIS cloud retrievals to Cloud-Aerosol LiDAR with Orthogonal Polarization and found that MODIS slightly overestimates liquid cloud fraction by $\sim$1%, but underestimates ice cloud fraction by approximately 5% in the Arctic. Therefore, we think that the selection of 1% and 3% for total cloud fraction is within current uncertainty estimates. We also increase cloud optical depth, shown in the third experiment (C3). Specifically, the uncorrected retrieved cloud optical depth is used in this experiment, which increases the cloud optical depth in the RTM calculation under high sea ice concentrations during the polar daytime. The fourth (C4) and fifth (C5) experiments simultaneously perturb cloud fraction (1% or 3%) and cloud optical depth.

3. The validation of CERES SYN1deg and EBAF products by MOSAiC surface measurements

First, we compare the time series of hourly surface radiative fluxes from MOSAiC ASFS30 (black) and SYN1deg-Hour (red) in **Figure 4**. In general, both SW and LW fluxes are well-aligned between the 2 data sets during April–September 2020. Note that the SW up flux in SYN1deg-Hour is generally smaller than that measured by the ASFS30 station. The LW down flux in SYN1deg-Hour is also smaller than the MOSAiC measurement, particularly from mid-August to late September. Similar results are found when we compare SYN1deg-Hour with ASFS50 and Met City (Figures S2 and S3).

The scatter plots and statistics comparing each radiative flux component are given in **Figure 5**. This figure shows that all components in SYN1deg-Hour exhibit very high correlations (>0.90) with the MOSAiC measurements except net longwave (LW net) fluxes, indicating an overall good agreement between the 2 data sets. Specifically, SYN1deg shows a bias (RMSE) of +11.40 (33.11) Wm^{-2} in SW down flux, which is about 7.70% of the mean observed value. Meanwhile, SYN1deg underestimates SW up flux by 15.70 Wm^{-2} and 15.18%, with the RMSE of 34.20 Wm^{-2}. A regression analysis has been performed between MOSAiC and CERES data, as shown in light blue in **Figure 5**. The regression results demonstrate that SW up has less agreement with MOSAiC than SW down, as the SW up slope is further away from one. In comparison, the biases (RMSEs) of longwave fluxes in SYN1deg are smaller, which are −12.58 (23.49) Wm^{-2} for LW down and −2.00 (8.72) Wm^{-2} for LW up. Both LW down and LW up have a regression slope around 0.9. It is interesting to note that there are large differences in LW up when the MOSAiC surface observations reach approximately 320 Wm^{-2} as SYN1deg has a wider distribution (300–330 Wm^{-2}) around this value, likely caused by differences in surface temperature data. This result is slightly different from Riihela et al. (2017), who concluded that the SYN1deg LW up flux over sea ice appears to saturate to approximately 315 Wm^{-2} during mid-summer corresponding to the sea ice melting point.

Combining the biases in both SW_down and SW_up, the SYN1deg shows a relatively large bias (RMSE) of +27.59 (38.03) Wm^{-2} for the SW_net flux and −10.53 (19.21) Wm^{-2} for the LW_net flux compared to MOSAiC. In terms of percentage, SYN1deg overestimates SW_net by 62.34%, but underestimates LW_net by 57.57%. The regression lines for both LW_net and SW_net show large differences with the identity line ($y = x$). As mentioned earlier, the point-by-point comparison in **Figure 5** is made

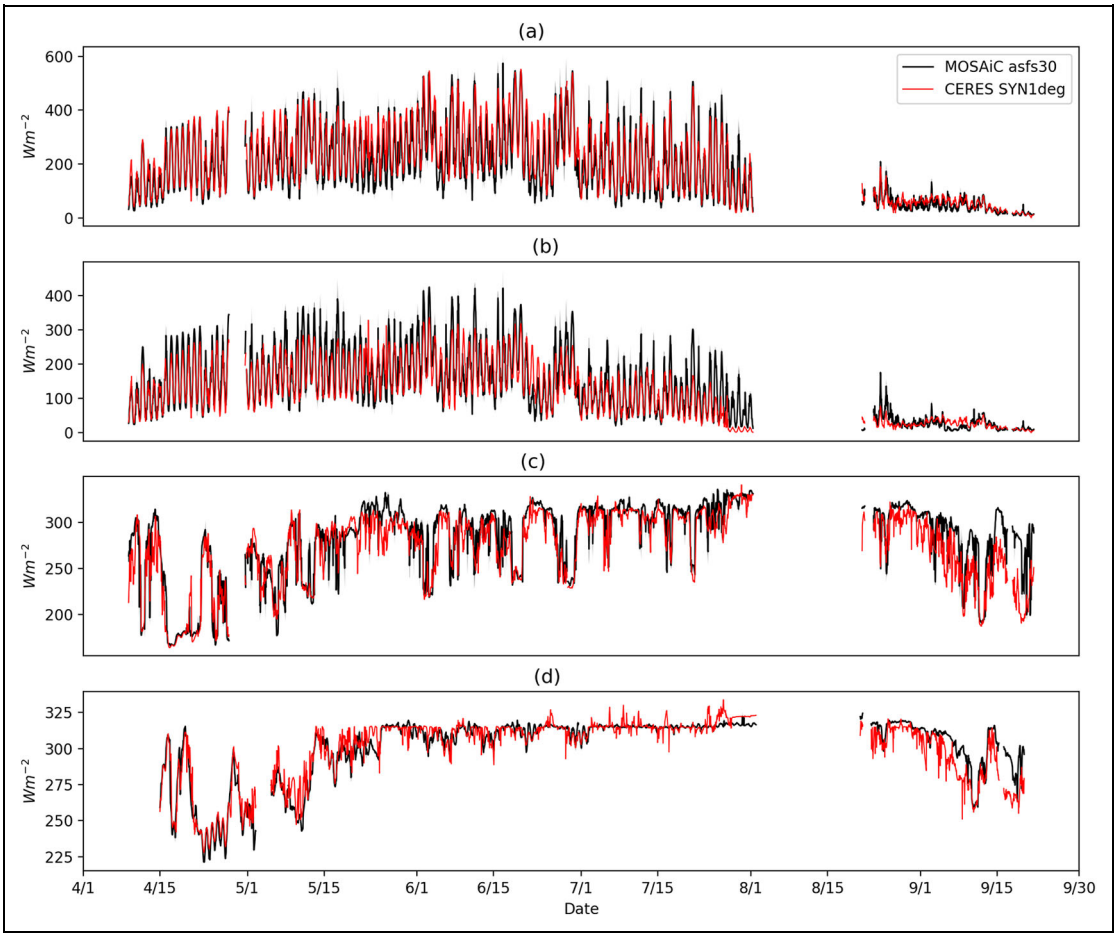

Figure 4. The time series of surface radiative fluxes for MOSAiC ASFS30 (black) and CERES SYN1deg (red) during April–September 2020 for (a) downward shortwave flux (SW_down), (b) upward shortwave flux (SW_up), (c) downward longwave flux (LW_down), and (d) upward longwave flux (LW_up). DOI: https://doi.org/10.1525/elementa.2022.00013.f4

between MOSAiC and SYN1deg only if there are at least 2 measurements available among ASFS30, ASFS50, and Met City. The statistical results for this subset of data are also consistent with the data from the individual measurement sites (Figure S5) suggesting that spatial heterogeneity in the MOSAiC measurements does not exert a large influence on the differences in shortwave and longwave fluxes between SYN1deg and MOSAiC. Further investigating the influence of spatial heterogeneity, we find weak relationships between the SYN1deg bias and spatial heterogeneity for all components except the SW_net flux (Figure S6). Recall that spatial heterogeneity variability is defined as the ratio (in percentage) between the absolute variance and the average of all available MOSAiC measurements. Of note is that the bias in SYN1deg SW_net tends to be smaller when a substantial spatial difference occurs in the MOSAiC measurements. In other words, SYN1deg has a better agreement with the MOSAiC observations under conditions of larger spatial heterogeneity, likely due to the larger spatial domain ($1^\circ \times 1^\circ$) of SYN1deg compared to MOSAiC point measurements. This result suggests that the 2 or 3 sites available during MOSAiC were insufficient to capture the full scale of spatial heterogeneity under all conditions.

The difference between CERES SYN1deg-Hour and MOSAiC measurements can be also attributed to CERES sampling as satellites view a larger domain including both ocean and sea ice. We quantify this effect by only including the CERES footprints with high sea ice concentration (>80%) in the comparison (Figure S7), resulting in approximately 70% of the points being kept. In general, there is no substantial difference between all points and the points with high sea ice concentrations except SW_up flux. Specifically, under high sea ice concentrations, the correlation of SW_up flux increased from 0.94 to 0.96, and both bias (from −15.70 to −10.96 Wm^{-2}) and RMSE (from 34.20 to 27.91 Wm^{-2}) reduced, demonstrating the influence of satellite versus surface-based sampling on SW_up flux bias. Similar issues can be found in surface broadband albedo comparison. The CERES surface albedo bias decreases slightly considering only sea ice concentrations >80% (**Figure 3**; described below).

Since SW_up flux from CERES SYN1deg-Hour shows the largest bias and RMSE relative to the MOSAiC measurements, we take a closer look at its differences in each individual month (**Figure 6**). In general, the SYN1deg-Hour and MOSAiC observations correlate better during April–July (>0.80) than in August and September. The very

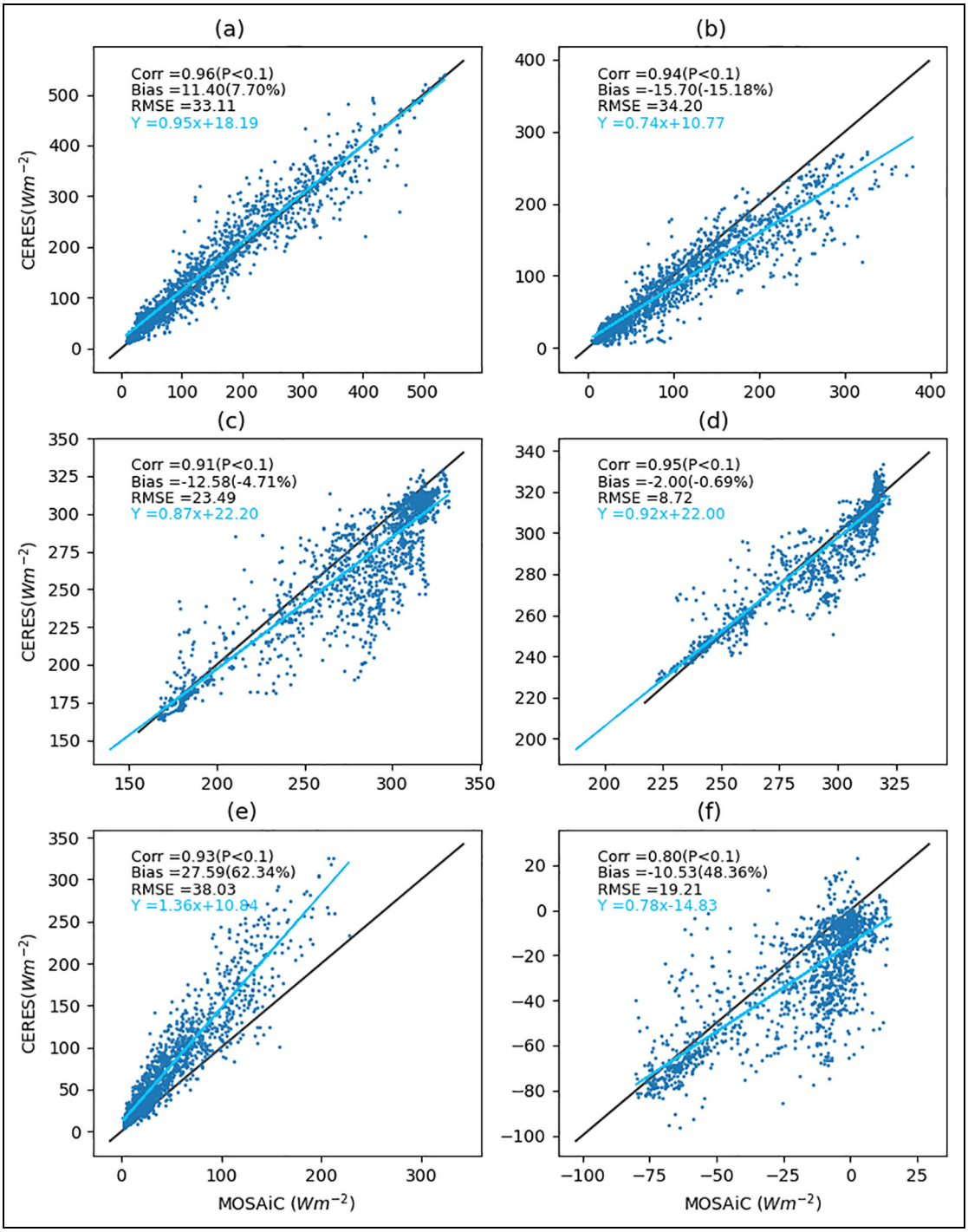

Figure 5. Comparison of surface radiative fluxes between MOSAiC ground observations and CERES SYN1deg during April–September 2020 for (a) downward shortwave flux (SW_down), (b) upward shortwave flux (SW_up), (c) downward longwave flux (LW_down), (d) upward longwave flux (LW_up), (e) net shortwave flux (SW_net), and (f) net longwave flux (LW_net). The correlation (Corr) with *P* value in parenthesis, absolute bias relative to the mean value of MOSAiC measurement (Bias) with relative bias (%) in parenthesis, root-mean-square error (RMSE), and regression equation are provided for each radiative flux component. A linear regression line is also provided (blue) to be compared with identity line ($y = x$, black). The point-by-point comparison is shown between MOSAiC observations and SYN1deg only if there are at least 2 measurements available among ASFS30, ASFS50, and Met City. The MOSAiC observations are obtained by averaging all available measurements at a given time. DOI: https://doi.org/10.1525/elementa.2022.00013.f5

low correlation (0.23) and large relative bias (–23.38%) in August are influenced by the smaller sample size and remain unchanged when considering only points with sea ice concentration greater than 80%. The more northerly grid points (approximately 85°N) in August and September may have an impact on the comparison, due to the

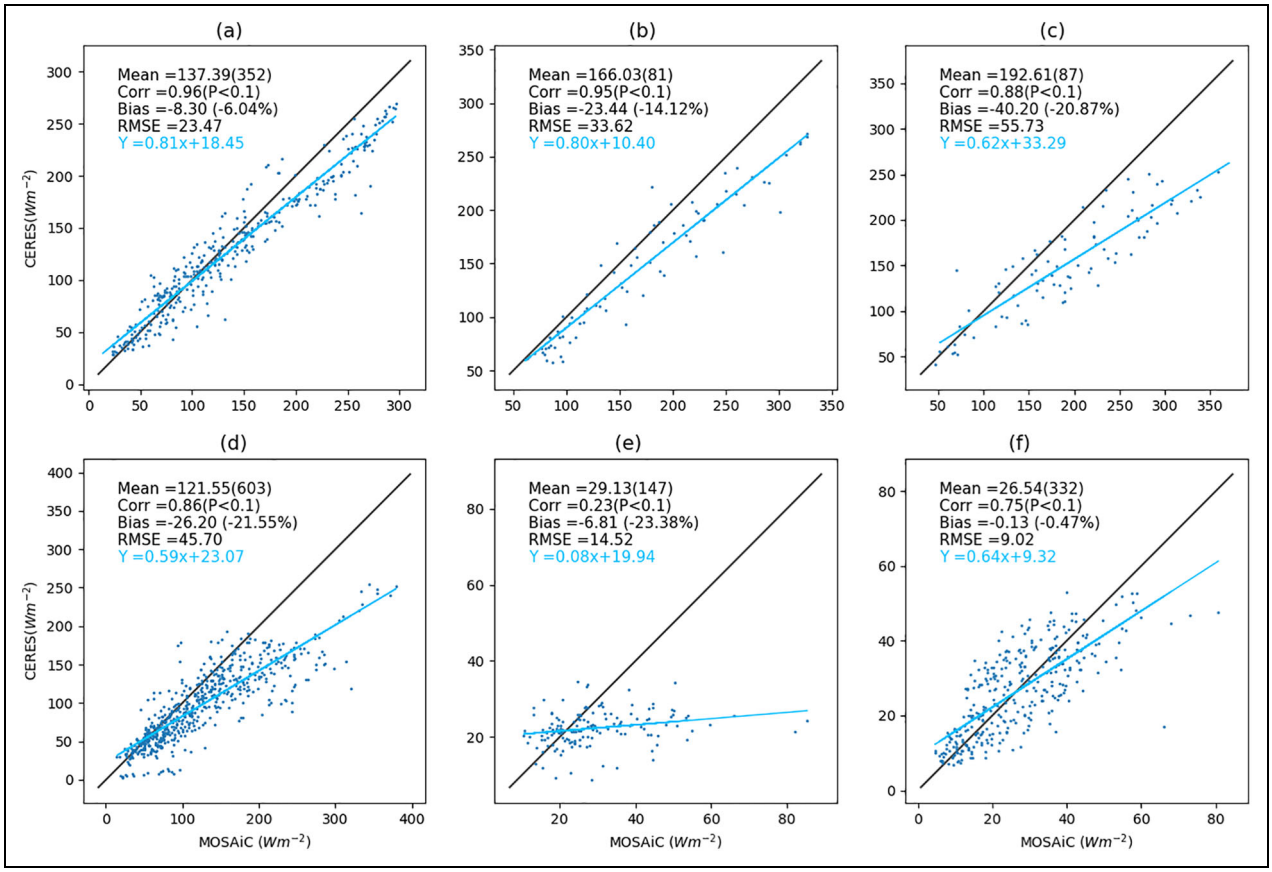

Figure 6. The monthly comparison of surface radiative fluxes between MOSAiC observations and CERES SYN1deg during (a) April to (f) September 2020 for upward shortwave flux (SW_up). The mean value (Mean) of MOSAiC measurements with sample size in parenthesis, correlation (Corr) with *P* value in parenthesis, absolute bias relative to the mean value of MOSAiC measurement (Bias) with relative bias (percentage) in parenthesis, root-mean-square error (RMSE) and regression equation are provided for each month. A linear regression line is also provided (blue) to be compared with identity line ($y = x$, black). DOI: https://doi.org/10.1525/elementa.2022.00013.f6

smaller solar radiation. Since the mean SW_up flux differs by month, it is more meaningful to compare the relative biases rather than absolute values. In this case, the largest relative biases occur in mid-summer and are smaller in late spring (April) and early fall (September) possibly related to greater surface albedo spatial heterogeneity in mid-summer.

In general, surface SW_down is biased high, and LW_down is biased low in CERES SYN1deg. These biases suggest that the atmosphere represented in the CERES product is too optically thin (e.g., too few clouds and/or too thin clouds). A complete exploration of satellite cloud property retrieval biases beyond the perturbation experiments in Section 4 and their influence on CERES surface radiative fluxes is beyond the scope of this analysis and will be addressed in future work.

Next, we quantify the sources of uncertainty in SYN1deg surface radiative fluxes by comparing several meteorological variables with available MOSAiC measurements (**Figure 7**). Note that these variables are used as inputs to calculate the SYN1deg radiative fluxes only. The surface albedo in SYN1deg-Hour is consistently lower than the MOSAiC flux station observations by 0.15 (–21.01%), with the RMSE of 0.17 and regression slope of 0.90 (**Figure 7a**), contributing substantially to the large negative bias in the SW_up flux (**Figure 5b**; see Section 4). Note that the SYN1deg surface albedo bias depends on sea ice concentration at 1°×1° grid scale. As shown in **Figure 3b**, the surface albedo bias decreases as the sea ice concentration increases, ranging from –0.43 to –0.10, due to the sampling differences between CERES and MOSAiC surface sites. Under high sea ice concentrations (>80%), the surface albedo biases are stable and remain between –0.10 and –0.14. This dependence on sea ice concentration is expected because the surface irradiance measurements represent the radiative fluxes over sea ice. Therefore, the differences are larger when we compare MOSAiC measurements with CERES grid boxes with high ocean fraction. The results are consistent with Riihela et al. (2017), where they found that SYN1deg surface albedo over sea ice is lower than the Tara drifting station measurements from April–June 2007. As in the surface radiative flux comparison, we consider these differences for only CERES footprints with high sea ice concentrations (>80%) (Figure S8). There is no substantial difference between all points and the points with high sea ice concentration. As

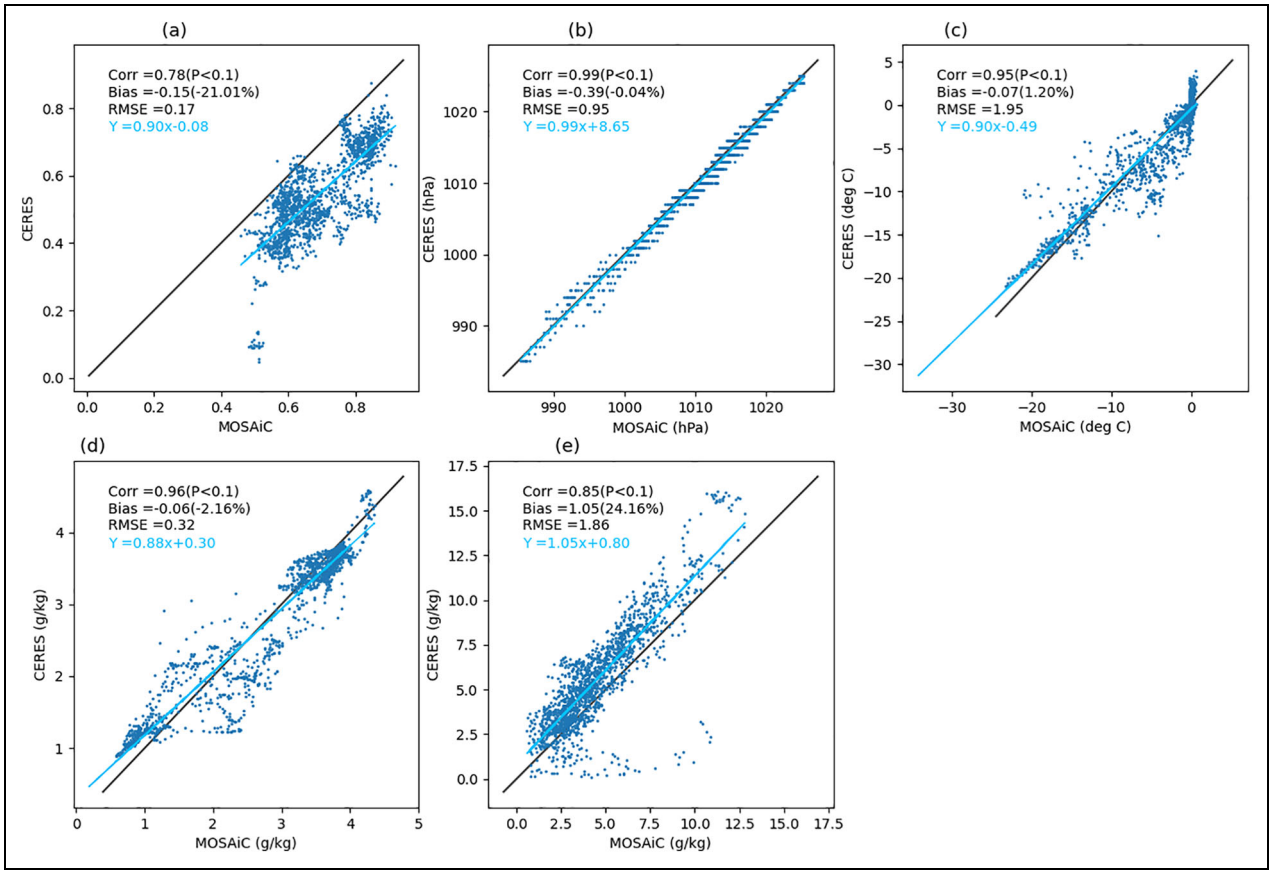

Figure 7. Comparison of CERES SYN1deg input to Fu–Liou radiative transfer model with MOSAiC surface measurements during April–September 2020 for (a) surface albedo, (b) surface pressure, (c) surface skin temperature, (d) surface water vapor mixing ratio, and (e) surface wind speed. The correlation (Corr) with *P* value in parenthesis, absolute bias relative to the mean value of MOSAiC measurement (Bias) with relative bias (percentage) in parenthesis, root-mean-square error (RMSE) and regression equations are provided for each variable. A linear regression line is also provided (blue) to be compared with identity line ($y = x$, black).The point-by-point comparison is shown between MOSAiC observations and SYN1deg only if there are at least two measurements available among ASFS30, ASFS50, and Met City. The MOSAiC observations are obtained by averaging all available measurements at a given time. DOI: https://doi.org/10.1525/elementa.2022.00013.f7

expected, the slight difference occurs for surface albedo. Due to sampling differences, both bias (from –0.15 to –0.14) and RMSE (from 0.17 to 0.16) in surface albedo are slightly reduced under high sea ice concentrations, while the correlation decreased from 0.78 to 0.75. In addition to sea ice concentration, snow and the presence of melt ponds in summertime also enhance the spatial heterogeneity of surface albedo, which further increases the uncertainties in comparison between satellite and surface measurements. We also compared the broadband albedo in SYN1deg-Hour with the one directly measured by MOSAiC survey line on a daily scale. As expected, a smaller difference (−0.09) is found in SYN1deg-Hour when compared to survey line, probably because the survey line contains more melt ponds than flux station.

We also compare the spectral shape of surface albedo between CERES and MOSAiC survey line measurements (**Figure 8**). Note that MOSAiC measured spectral albedo is only available during June–September 2020. Overall, the CERES spectral albedo (0.7–0.8) is larger than that of MOSAiC within the visible band (0.3–0.7 μm) by 0.1–0.2 and mid-infrared band (>1.5 μm) by approximately 0.1, while lower than MOSAiC within the near-infrared band (0.7 −1.4 μm) by 0.0–0.3. The monthly averaged spectral albedo shows similar patterns except July, during which the CERES spectral albedo is lower than MOSAiC by approximately 0.1 within the visible band. Recall that CERES broadband albedo is lower than that measured by the MOSAiC flux stations.

The surface pressure in SYN1deg agrees well with the one measured by MOSAiC, with a positive correlation of 0.99 and a slightly negative bias of –0.39 hPa (–0.04%). The surface skin temperatures measurements from MOSAiC are derived from surface upwelling and downwelling longwave fluxes assuming a surface emissivity of 0.985 (Persson et al., 2002; **Figure 7c**). The SYN1deg underestimates surface skin temperature by –0.07°C (–1.20%) compared with the MOSAiC measurements. As expected, there are large differences in surface skin temperature when the surface reaches melting point, which contributes to biases in LW_up flux when it is around 320 Wm^{-2} (**Figure 5d**). A similar issue is found in LW_net

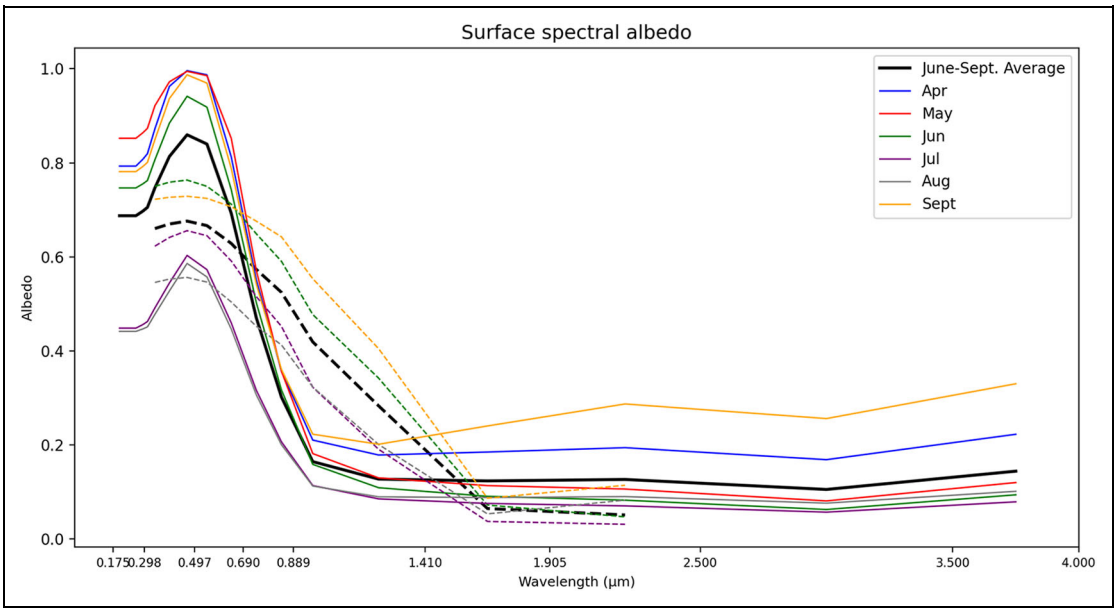

Figure 8. The surface spectral albedo in CERES-like radiative transfer model control run (solid line) and MOSAiC (dashed line) for each month during April–September 2020. Note that the MOSAiC measured spectral albedo is only available during June–September. The black lines represent June–September averaged spectral albedo. DOI: https://doi.org/10.1525/elementa.2022.00013.f8

flux (**Figure 5f**), as SYN1deg has a wide distribution when MOSAiC reaches 0 Wm^{-2}. This result is influenced by the larger spatial domain of CERES; that is, CERES SYN1deg data includes more heterogenous scenes with temperature values that represent the average of ice-free ocean and sea ice portions of the grid box. Depending on salinity, the freezing point of ocean water is between 0°C (fresh) and −1.8°C (typical salty), while it should be 0°C for fresh snow on sea ice. Therefore, compared to MOSAiC ice-only point measurements, a larger spatial domain in SYN1deg would result in temperature differences since it contains both ice and ocean. The MOSAiC observations also indicate little variability in the broadband surface emissivity during the measurement period. **Figure 7d** shows a good agreement of the surface water vapor mixing ratio between the 2 datasets, with a slightly negative bias of −0.06 g/kg (−2.16%) in SYN1deg. A more thorough validation of SYN1deg longwave fluxes is needed once the vertical profiles of water vapor become available from the MOSAiC field campaign. The GOES-5.4.1 simulated wind speed, which partially determines the surface spectral albedo, exhibits a positive bias of 1.05 m/s (24.16%) and RMSE of 1.86 m/s compared to MOSAiC measurements. However, the wind speed is only one of several factors determining the initial spectral albedo LUTs and exerts very little impact on the radiative fluxes.

The results above are based on the comparison between SYN1deg-Hour and MOSAiC surface observations. Given that the CERES EBAF is a widely used product to evaluate most of the Coupled Model Intercomparison Project Phase 5/6 climate models (e.g., Wild et al., 2015; Dolinar et al., 2015; Boeke and Taylor, 2016; Baker and Taylor, 2016; Wild, 2020), it is worthwhile to investigate how the biases in CERES hourly products are transferred to EBAF monthly products. Therefore, CERES SYN1deg-Hour (blue), SYN1deg-Month (green), and EBAF (red) products are compared with MOSAiC measurements and shown in **Figure 9**. As for shortwave fluxes, EBAF shows the smallest overall bias among the 3 products, with a bias of +6.54 Wm^{-2} for SW_down flux and −11.51 Wm^{-2} for SW_up flux. Riihela et al. (2017) also found a reduced underestimation of SW_up flux in EBAF compared to SYN1 deg. As for the LW_down flux, EBAF contains the largest bias for almost all 6 months, with the overall bias −12.31 Wm^{-2} (−4.36%). The overall bias of LW_up flux in EBAF, however, is smaller than from SYN1deg-Hour and SYN1deg-Month products (**Figure 9d**). The overall small bias for EBAF is due to compensating effects of large positive biases in May and June and negative biases in April and September. In addition, the SW_net flux bias in EBAF is smaller than that in SYN1deg-Month for all months except September. The overall positive bias in EBAF has been reduced by 15% compared with SYN1deg-Month. In comparison, the LW_net bias in EBAF increased by approximately 20% relative to SYN1deg-Month, particularly in May, June, and July.

The similar comparison between CERES products and MOSAiC is also done for surface albedo shown in **Figure 10**. Here, we compare the monthly *Terra* (purple) and *Aqua* SAH (yellow). The CERES EBAF shows the best agreement with MOSAiC surface measurements from April to September, with a minimum bias of −0.08 (−11.29%) among all products. In addition, the negative biases (−0.14) in SYN1deg-Hour and SYN1deg-Month are larger than that in *Terra* (−0.10) and *Aqua* SAH (−0.13). Differences between *Terra* and *Aqua* SAH, however, are primarily attributed to satellite sampling in the polar regions (Rutan et al., 2009). Overall, the CERES EBAF

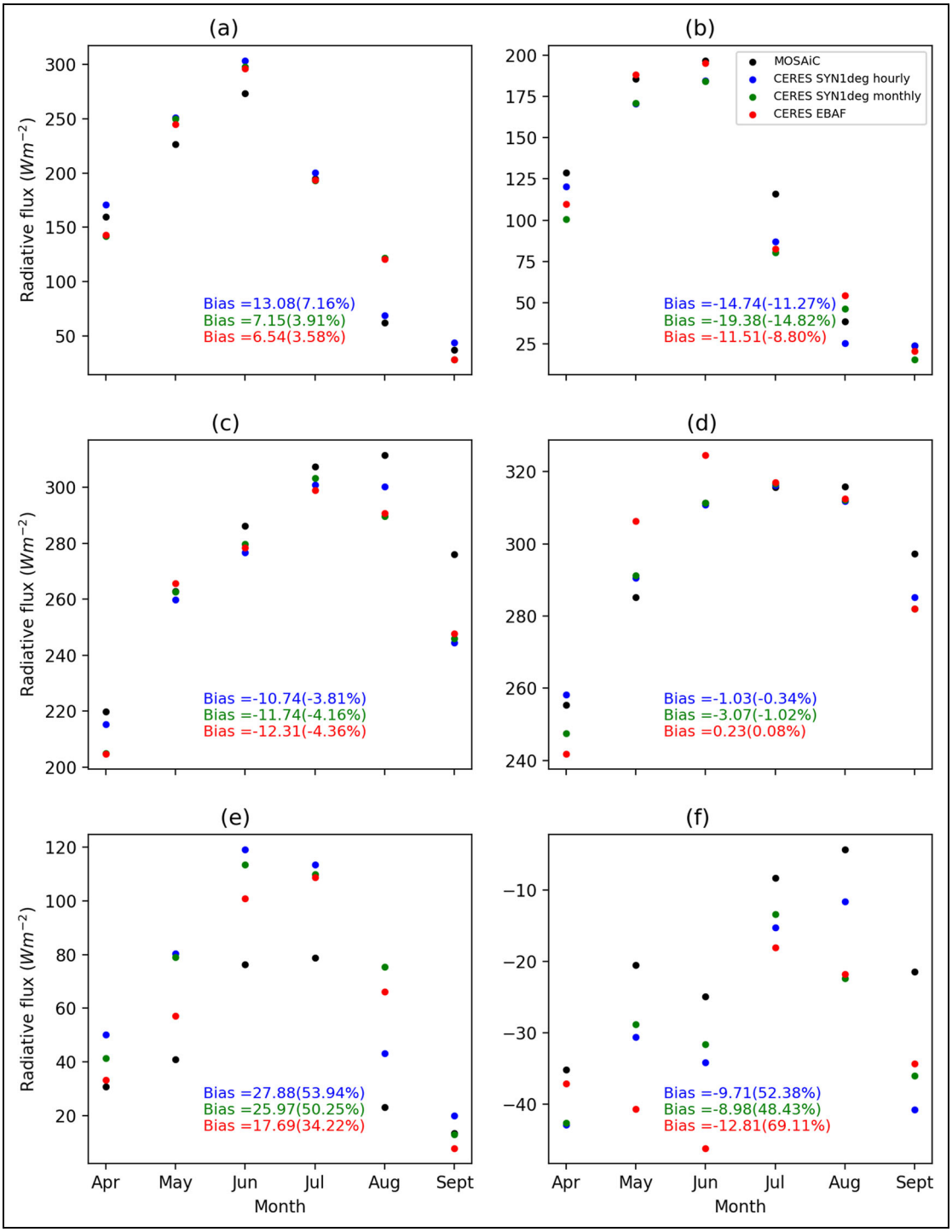

Figure 9. The monthly surface radiative fluxes obtained from MOSAiC observations (black), CERES SYN1deg (blue), and CERES EBAF (red) during April–September 2020 for (a) downward shortwave flux (SW_down), (b) upward shortwave flux (SW_up), (c) downward longwave flux (LW_down), (d) upward longwave flux (LW_up), € net shortwave flux (SW_net), and (f) net longwave flux (LW_net). The absolute bias relative to the mean value of the MOSAiC measurements, with relative bias (%) in parenthesis are provided for each radiative flux component and each product, which are calculated from all collocated hourly data points. DOI: https://doi.org/10.1525/elementa.2022.00013.f9

improves from SYN1deg products in terms of shortwave fluxes and surface albedo through the bias correction and Lagrange multiplier to the SYN1deg-Month product (Kato et al., 2018). However, the EBAF longwave fluxes show larger biases compared with SYN1deg-Month. Contributing to these larger longwave biases are likely the large uncertainties in Arctic temperature measurements in the bias correction process and the disconnected nature of TOA and surface fluxes due to frequent occurrence of temperature inversions that would inhibit the ability to constrain surface fluxes with TOA flux measurements.

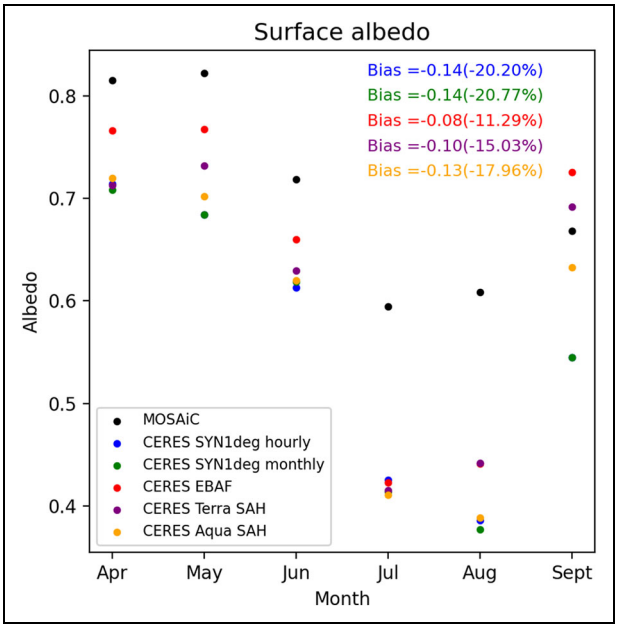

Figure 10. Same as Figure 9, but for surface albedo. DOI: https://doi.org/10.1525/elementa.2022.00013.f10

4. Perturbation experiments with RTM

4.1. Surface albedo perturbation experiments

The analyses above demonstrate that surface albedo significantly contributes to the large negative bias in SW_up flux in CERES SYN1deg products. Therefore, we perform CERES-like RTM calculations, replacing the CERES surface albedo with other approximations of this parameter to quantify its contribution to the SYN1deg bias.

Different strategies are used to perturb either SAH_hourly or SAH_monthly. **Table 4** shows the difference relative to the mean value from MOSAiC measurements (in percentage) for each radiative flux component in various RTM perturbation experiments. As a result of most perturbations, the magnitude of the bias in SW_up flux is substantially reduced compared to the control run, which is −14.14% relative to MOSAiC observations. Concurrently, the bias in SW_down flux is increased from +4.31%, reaching 7%–10%, which can be explained by enhanced multiple reflections between clouds and the highly reflective surface (e.g., Wendler et al., 2004). There are no changes in either LW_down or LW_up with perturbed broadband surface albedo. The A1 experiment, using the observed hourly broadband albedo, shows a large change in the SW_up flux (+15.28%) and the largest change in SW_down flux (+5.27%) relative to the control run. This improvement can also be demonstrated by the regression analysis, as the slope increases from 0.82 (control run) to 0.87 (A1) for SW_up (Fig. S9). As expected, changes are smaller in SW fluxes when we adjust the SAH at monthly scale (A2); the differences between A1 and A2 stem from high frequency variability in surface albedo that is not accounted for when modeling daily surface albedo variability using sea ice concentration anomalies as is assumed in the CERES SYN process (**Figure 2**). This result suggests that surface albedo variability that cannot be explained by sea ice concentration variations (e.g., snow, melt ponds) accounts for approximately 4 W m^{-2} (+0.10–0.22) of the negative bias in the SW_up flux. A3 and A4 represent more feasible correction approaches in the SAH data; we correct SAH_monthly by either a single constant during summer (+0.15) or different values for each month. The changes in SW_up in A3 (+16.02%) and A4 (+16.82%) are close to A1, while the bias in SW_down is smaller by approximately 1%. It should be noted that A3 exhibits the smallest bias in SW_net (+25.73%) among all experiments. The last broadband surface albedo perturbation experiment A5 shows a similar change in SW_net (−22.15%) compared to A1, with a smaller change in both SW_down and SW_up. Specifically, the bias (RMSE) for SW_down and SW_up in A5 are +14.71 (44.00) Wm^{-2} and −0.24 (33.55) Wm^{-2}, respectively (**Table 5**). Overall, the bias (RMSE) of the SW_net flux decreased to +14.99 (28.68) Wm^{-2} from +26.44 (38.69) Wm^{-2} in the control run. Experiment A5 is believed to be the most appropriate method because the surface albedo adjustment is scaled by the sea ice concentration in each 1°×1° grid box to account for CERES and MOSAiC sampling differences (Section 2.4).

Since the MOSAiC measurements are mostly over sea ice, we also compare the results from all perturbation experiments using all data points and just those points with high sea ice concentrations (>80%; Table S1). In general, the agreement in SW_up flux is slightly improved under high sea ice concentrations in most perturbation experiments. As for SW_down flux, the bias is increased in all perturbation experiments except A1, which means that fundamental issues remain in how the atmosphere is treated (i.e., the atmosphere is too optically thin or there are too few clouds) in the satellite-based retrieval process.

To quantify the impacts of albedo spectral shape on the shortwave flux bias, we run 2 additional experiments, A6 and A7, by replacing initial spectral albedo with monthly averaged spectral albedo obtained from the RTM control run and MOSAiC spectral albedo, respectively. Experiment A7 should only be compared directly with A6 because these calculations are made only for June–September, not the entire melt season. As mentioned earlier, the CERES albedo is larger than MOSAiC within the visible band (0.3–0.7 μm) and mid-SW infrared band (>1.5 μm), while smaller than MOSAiC within the shortwave near-infrared band (0.7 −1.4 μm). By using the MOSAiC spectral albedo, the SW_up flux bias becomes more negative by 2.61% or −2.93 Wm^{-2} compared to Experiment A6, which uses the CERES spectral albedo. Additionally, this change in the spectral albedo shape results in a closer agreement in the SW_down flux, with a change of −1.02% and −1.76 Wm^{-2} relative to A6. Using the MOSAiC spectral albedo gives a more negative SW_up flux bias, which is opposite to the less negative value derived by replacing with MOSAiC broadband albedo. First, these results may suggest that the underestimation of broadband albedo is partially compensated by the overestimation of spectral albedo in visible bands in the CERES SYN1deg product. Second, the integration of spectral albedo from the MOSAiC survey line may not be comparable with broadband albedo

Table 4. The relative bias to the mean value (in %) from Multidisciplinary drifting Observatory for the Study of Arctic Climate (MOSAiC) measurements in Fu–Liou radiative transfer model control run and surface albedo perturbation runs. DOI: https://doi.org/10.1525/elementa.2022.00013.t4

Experiment	SW_down (%)	SW_up (%)	SW_net (%)	LW_down (%)	LW_net (%)
Control run	+4.31	−14.14	+51.2	−2.51	−34.8
A1—"True" SAH_hourly	+9.58 (+5.27)	+1.14 (+15.3)	+31.0 (−20.1)	−2.51 (0.00)	−34.8 (N/A)
A2—"True" SAH_monthly	+7.86 (+3.55)	−1.75 (+12.4)	+32.3 (−18.8)	−2.51 (0.00)	−34.8 (N/A)
A3—correction to SAH_monthly by a constant in summer	+8.61 (+4.30)	+1.88 (+16.0)	+25.7 (−25.4)	−2.51 (0.00)	−34.8 (N/A)
A4—correction to SAH_monthly by a constant for each month	+8.88 (+4.57)	+2.68 (+16.8)	+26.7 (−24.5)	−2.51 (0.00)	−34.8 (N/A)
A5—correction to SAH_monthly by weighted surface albedo for each sea ice bin	+8.05 (+3.74)	−0.18 (+14.0)	+29.0 (−22.2)	−2.51 (0.00)	−34.8 (N/A)
A6—monthly averaged spectral albedo from control run (June–September)	+6.38 (N/A)	−13.5 (N/A)	+44.4 (N/A)	−3.21 (N/A)	+44.1 (N/A)
A7—monthly averaged spectral albedo from MOSAiC (June–September)	+5.36 (−1.02)	−16.1 (−2.61)	+46.4 (+2.00)	−3.21 (0.00)	+44.1 (0.00)

The changes relative to control run in each perturbation run is provided in parentheses. Note that the values in parentheses for Experiment A7 are the relative changes to A6. SW_down = downward shortwave flux; SW_up = upward shortwave flux; SW_net = net shortwave flux; LW_down = downward longwave flux; LW_net = net longwave flux.

Table 5. The biases (in Wm^{-2}) of surface shortwave fluxes in Fu–Liou radiative transfer model control run and surface albedo perturbation runs relative to the Multidisciplinary drifting Observatory for the Study of Arctic Climate (MOSAiC) measurements. DOI: https://doi.org/10.1525/elementa.2022.00013.t5

Experiment	SW_down		SW_up		SW_net	
Error Type	Bias	RMSE	Bias	RMSE	Bias	RMSE
Control run	+7.88	41.5	−18.5	38.3	+26.4	38.7
A1	+17.5	45.1	+1.49	32.6	+16.0	27.7
A2	+14.4	43.7	−2.29	32.3	+16.7	28.7
A3	+15.7	44.5	+2.46	33.9	+13.3	27.5
A4	+16.2	44.8	+3.50	34.5	+12.7	27.1
A5	+14.7	44.0	−0.24	33.6	+15.0	28.7
A6	+11.0	44.1	−15.1	37.8	+26.1	40.5
A7	+9.19	42.9	−18.0	38.7	+27.3	42.0

All the values are in W m^{-2}. SW_down = downward shortwave flux; SW_up = upward shortwave flux; SW_net = net shortwave flux.

measurements from the flux station due to inconsistent spectral ranges. Further, it is possible that the survey line samples contain more ponded sea ice than the flux station, which could contribute to these differences in the broadband/spectral albedo comparisons. In terms of SW_up flux, differences in the spectral albedo shape between CERES and observations suggest an approximately 3 W m^{-2} effect (A6 and A7), whereas the broadband albedo differences are an approximately 20 W m^{-2} effect (A5 and control run). In this case, the difference in CERES broadband albedo makes a larger contribution to the uncertainty in SW_up flux than spectral albedo shape. However, it should be noted that only a specific spectral range was measured by MOSAiC, which is expected to have only a minor impact on these results.

4.2. Cloud perturbation experiments

The SW_down flux bias increased with the increased surface albedo in each perturbation experiment. This increase can be attributed to the brightening of the surface and an increase in multiple reflections between clouds and surface. As mentioned earlier, the SW_down flux is biased high and LW_down flux is biased low, suggesting that there might be too few clouds and/or too thin clouds. In response to this finding, we perform a series of cloud perturbation experiments on top of the

A5 surface albedo changes to estimate the magnitude of the cloud property changes required to offset this bias (see **Table 3**).

Table 6 shows the percentage bias relative to mean observed values for each radiative flux component, while **Table 7** provides bias and RMSE in units of Wm^{-2} in each experiment relative to MOSAiC measurements. Compared to the albedo perturbation Experiment A5, the bias in SW_down flux has been slightly decreased to $+14.23$ Wm^{-2} (7.79%) and $+13.67$ Wm^{-2} (7.48%) when the cloud fraction is increased by 1% and 3%, respectively. Therefore, as cloud fraction increases, the bias in SW_down flux decreases, while the SW_up bias increases in (negative) magnitude. The effects of the 1% and 3% cloud fraction perturbations are small. Overall, the SW_net flux biases in both experiments slightly decreased, which is considered as an improvement from A5. It is interesting to note that the biases of LW_down and LW_net were slightly reduced in C1 and C2.

The third cloud perturbation experiment (C3), which increases the natural log of the polar daytime cloud optical depth by one, exhibits much larger changes in both shortwave and longwave fluxes. Specifically, the bias in SW_net flux decreased to $+10.69$ Wm^{-2} ($+20.68\%$) from $+14.99$ Wm^{-2} ($+29.00\%$) in Experiment A5, with the bias in SW_down flux of $+5.14$ Wm^{-2} (2.81%). Similarly, the bias in LW_net flux was reduced by more than half to -14.49%, due to the improvement in LW_down flux. As expected, the fourth (C4) and fifth (C5) experiments show the minimum biases in both SW net and LW net fluxes, as they increase both cloud fraction and cloud optical depth. Among the 5 experiments, C5 exhibits the closest agreement with the MOSAiC measurements, with biases in SW_net flux of $+10.29$ Wm^{-2} ($+19.90\%$) and LW_net flux of -5.97 Wm^{-2} (-10.53%). The results from all CERES-like RTM perturbation experiments demonstrate that the biases in both SYN1deg shortwave and longwave fluxes can be substantially reduced by correcting albedo and

Table 6. The relative bias to the mean value (in %) from Multidisciplinary drifting Observatory for the Study of Arctic Climate (MOSAiC) measurements in Fu–Liou radiative transfer model control run and cloud perturbation runs. DOI: https://doi.org/10.1525/elementa.2022.00013.t6

Experiment	SW_down (%)	SW_up (%)	SW_net (%)	LW_down (%)	LW_net (%)
Control run	+4.31	−14.1	+51.2	−2.51	−34.8
A5—correction by a constant for each month	+8.05	−0.18	+29.0	−2.51	−34.8
C1—increase cloud fraction by 1%	+7.79	−0.43	+28.7	−2.41	−33.2
C2—increase cloud fraction by 3%	+7.48	−0.71	+28.3	−2.28	−31.3
C3—uncorrected retrieved cloud optical depth is being used	+2.81	−4.22	+20.7	−1.15	−14.5
C4—combine C1 and C3	+2.52	−4.48	+20.3	−1.04	−12.8
C5—combine C2 and C3	+2.17	−4.80	+19.9	−0.89	−10.5

The relative change in each perturbation run to control run is provided in parenthesis. SW_down = downward shortwave flux; SW_up = upward shortwave flux; SW_net = net shortwave flux; LW_down = downward longwave flux; LW_net = net longwave flux.

Table 7. The biases (in Wm^{-2}) of surface shortwave fluxes in Fu–Liou radiative transfer model control run and perturbation runs relative to the Multidisciplinary drifting Observatory for the Study of Arctic Climate (MOSAiC) measurements. DOI: https://doi.org/10.1525/elementa.2022.00013.t7

Experiment	SW_down		SW_up		SW_net		LW_down		LW_net	
Error Type	Bias	RMSE	Bias	RMSE	Bias	RMSE	Bias	RMSE	Bias	RMSE
Control run	+7.88	41.5	−18.5	38.3	+26.4	38.7	−7.09	19.5	−6.45	16.6
A5	+14.7	44.0	−0.24	33.6	+15.0	28.7	−7.93	20.5	−7.05	17.1
C1	+14.2	43.9	−0.56	33.6	+14.8	28.5	−6.80	19.4	−6.16	16.5
C2	+13.7	43.7	−0.93	33.7	+14.6	28.4	−6.43	19.3	−5.80	16.5
C3	+5.14	39.6	−5.51	33.4	+10.7	25.6	−3.25	16.8	−2.69	14.8
C4	+4.60	39.5	−5.86	33.5	+10.5	25.5	−2.92	16.8	−2.37	14.8
C5	+3.97	39.5	−6.28	33.6	+10.3	25.3	−6.60	19.4	−5.97	16.5

All the values are in W m^{-2}. SW_down = downward shortwave flux; SW_up = upward shortwave flux; SW_net = net shortwave flux; LW_down = downward longwave flux; LW_net = net longwave flux.

cloud biases together and that correcting only surface albedo worsens the agreement in SW down flux between CERES and MOSAiC.

The reduction in the SW_down bias is small due to adjusting the cloud properties, especially in C1 and C2. By increasing surface albedo and clouds simultaneously, the multiple reflections are expected to be stronger than when increasing surface albedo alone. The failure of the constant cloud fraction and cloud optical depth corrections to simultaneously account for the SW_down and SW_up biases indicates that errors in the MODIS cloud property retrievals depend upon the specific conditions. Yost et al. (2020) showed that compared to active-sensor data CloudSat and CALIPSO, several MODIS-retrieved cloud properties show the largest difference in polar regions. In addition to cloud fraction and optical depth, other cloud properties, such as vertical structure and cloud phase may play a role, and the RTM solver could also influence the surface radiative flux biases. Thus, a more sophisticated, condition dependent approach is needed to account for MODIS cloud property retrieval biases in order to resolve the SW flux biases. It is also important to note that the cloud treatment may not be the only contributing factor to the CERES SW biases; the unrealistic representation of other atmospheric conditions (e.g., water vapor vertical profiles) could also play a role.

5. Summary and conclusions

It is well known that uncertainty in CERES-derived irradiances is substantially larger over sea ice than any other surface. The year-long MOSAiC expedition has provided unprecedented observations of the Arctic and so allows for a much more complete uncertainty analysis of CERES radiative fluxes based on well calibrated surface observations.

First, a systematic and statistically robust assessment of surface shortwave and longwave fluxes was conducted using in situ measurements from MOSAiC in the Arctic ice pack. The CERES SYN1deg product overestimates the SW_down flux (+11.40 Wm^{-2}/+7.70%) as well as underestimates the SW_up (−15.70 Wm^{-2}/−15.18%) and LW_down fluxes (−12.58 Wm^{-2}/−4.71%) at the surface during summer. In addition, large differences in LW_up flux (approximately 320 Wm^{-2}) occur when the surface reaches the melting point (approximately 0°C), which can be explained by the errors in surface skin temperature obtained from GEOS-5.4.1 and the larger heterogeneity of satellite footprints compared to the ground-based in situ observations. The large negative bias in the SW_up flux can be attributed to the underestimation of surface albedo in SYN1deg-Hour. Specifically, the surface albedo in SYN1deg-Hour is consistently lower than that of MOSAiC by 0.15 (−21.01%). While sampling differences between CERES and MOSAiC in situ measurements can contribute to differences, results considering only CERES grid boxes with high sea ice concentrations (>80%) to minimize sampling differences show a similar surface albedo underestimation (−0.14).

In addition to a direct comparison, we performed a series of RTM perturbation experiments to quantify contributions to uncertainty. Different strategies are used to perturb SAH_hourly or SAH_monthly. In general, the bias in the SW_up flux is substantially reduced in these perturbation experiments relative to the control run, which showed a −14.14% bias relative to the MOSAiC observations. Concurrently, in these perturbation experiments, the bias in SW_down flux is increased, ranging from 7% to 10%, due to enhanced multiple reflections between clouds and the more reflective surface. The results with the closest agreement to MOSAiC observations are obtained by adjusting the CERES surface albedo input with a constant value proportional to sea ice concentration within each $1^\circ \times 1^\circ$ grid box. Specifically, the bias (RMSE) for the SW_down and SW_up fluxes in this experiment (A5) are +14.71 (44.00) Wm^{-2} and −0.24 (33.55) Wm^{-2}, respectively. Overall, the bias (RMSE) of the SW_net flux in this A5 experiment decreased to +14.99 (28.68) from +26.44 (38.69) Wm^{-2} in the control run. In addition, a compensating effect between underestimation of broadband albedo and overestimation of spectral albedo in visible and mid-infrared bands in SYN1deg datasets is found and contributes to the shortwave flux differences. The difference in CERES broadband albedo (approximately 20 Wm^{-2}) contributes to larger uncertainty in SW_up flux than spectral albedo shape (approximately 3 Wm^{-2}).

Moreover, the positive bias in SW_down flux and the negative bias in LW_down flux suggest that the atmosphere represented in the CERES product might be too optically thin. Therefore, another set of perturbation experiments was performed that simultaneously modified the cloud inputs and surface albedo. Particularly, the experiment (C5) that increased cloud fraction by 3% and the natural log of cloud optical depth by one, along with the adjustment to sea ice albedo from the A5 experiment, exhibited the best results among the 5 cloud experiments. The bias in the SW_net flux of +19.90% and the LW_net flux of −10.53% represent reductions of more than half compared to the control run. The results from all CERES-like RTM perturbation experiments demonstrate that biases in both SYN1deg shortwave and longwave fluxes must be addressed by correcting albedo and cloud biases together. Thus, when correcting for errors in the surface albedo, one must also simultaneously correct for biases in cloud properties.

This study focuses on surface radiative fluxes during summertime. We plan to extend our study to the full year observing period, although the uncertainty in satellite retrieved cloud and radiation properties is expected to be larger in winter than in summer. Longwave radiation dominates the Arctic surface energy budget for almost one-half of the year when insolation is absent or weak; therefore, it is extremely important for the Arctic system year-round (Curry et al., 1996; Marty et al., 2003). The MOSAiC field campaign offers a unique opportunity to assess surface longwave observations in winter. Furthermore, the differences between CERES-MODIS cloud properties and MOSAiC can be identified once MOSAiC cloud observations become available, facilitating additional RTM perturbation experiments with more representative cloud uncertainties. In

addition, the uncertainties in surface radiative fluxes from satellite measurements come from other sources. Note that some atmospheric and surface measurements from MOSAiC are still being processed and undergoing quality control. In the future, we plan to perform a radiation budget closure study using the available thermodynamic, surface, and cloud information collected aboard the *Polarstern* and at extended sites. Overall, the results can effectively inform the future development of CERES products, particularly in the polar regions. The goal of this project is to reduce uncertainties in the Arctic surface radiation budget derived from satellite measurements, which will greatly benefit the Arctic climate science community.

Data accessibility statement

In this study, NASA CERES SYN1deg (doi: 10.5067/TERRA+AQUA/CERES/SYN1DEG-1HOUR_L3.004A) and CERES EBAF-surface (doi: 10.5067/Terra-Aqua/CERES/EBAF_L3B.004.1) data sets are available at http://ceres.larc.nasa.gov/order_data.php. Data used in this article were produced as part of the international Multidisciplinary drifting Observatory for the Study of the Arctic Climate (MOSAiC) with the tag MOSAiC20192020 and the Project _ID: AWI_PS122_00. A subset of data was obtained from the Atmospheric Radiation Measurement (ARM) User Facility, a U.S. Department of Energy (DOE) Office of Science User Facility Managed by the Biological and Environmental Research Program. Surface radiation and near-surface meteorology measurements from the University of Colorado/NOAA surface flux team are available at the Arctic Data Center (Cox et al., 2021a; Cox et al., 2021b; Cox et al., 2021c; Cox et al., 2021d). Surface radiation at Met City from the ARM Program are available at the ARM archive (Riihimaki, 2021). MOSAiC spectral and broadband albedo data from survey line are archived in the MOSAiC Central Storage and can be accessed from the National Science Foundation's Arctic Data Center (Smith et al., 2021a; Smith et al., 2021b).

Supplemental files

The supplemental files for this article can be found as follows:

This research includes supplementary material (Tables S1, Figures S1–S9) that has been uploaded separately to this document.

Acknowledgment

We thank all people involved in the expedition of the Research Vessel *Polarstern* during MOSAiC field campaign in 2019–2020 as listed in Nixdorf et al. (2021).

Funding

This study was supported by NASA Radiation Budget Science Project. MAW conducted this work under NASA's New Investigator Program in Earth Science (80NSSC 20K0658) and Interdisciplinary Research in Earth Science program (80NSSC21K0264). MDS was supported by the National Science Foundation (OPP-1724551), U.S. Department of Energy (DOE) Atmospheric System Research Program (DE-SC0019251, DE-SC0021341), and the NOAA Physical Sciences Laboratory and Global Ocean Monitoring and Observing Program. MMS was supported by the National Science Foundation (OPP-1724467 and OPP-1724748).

Competing interests

The authors declare that they have no competing interests.

Author contributions

Led the conception and design of study: YH, PCT.

Conducted the field work: MDS, MAW, MMS.

Contributed to the acquisition of data: FGR, DAR, MDS, MAW, MMS.

Contributed to analysis and interpretation of data: All authors.

Drafted and/or revised the article: All authors.

Approved the submitted version for publication: All authors.

References

Baker, NC, **Taylor, PC**. 2016. A framework for evaluating climate model performance metrics. *Journal of Climate* **29**: 1773–1782. DOI: https://dx.doi.org/10/1175/JCLI-D-15-0114.1.

Boeke, RC, **Taylor, PC**. 2016. Evaluation of the Arctic surface radiation budget in CMIP5 models. *Journal of Geophysical Research: Atmospheres* **121**(14): 8525–8548. DOI: https://dx.doi.org/10.1002/2016JD025099.

Boos, WR, **Korty, RL**. 2016. Regional energy budget control of the intertropical convergence zone and application to mid-Holocene rainfall. *Nature Geoscience* **9**(12): 892–897. DOI: https://www.nature.com/articles/ngeo2833.

Briegleb, BP, **Minnis, P**, **Ramanathan, V**, **Harrison, E**. 1986. Comparison of regional clear-sky albedos inferred from satellite observations and model computations. *Journal of Applied Meteorology and Climatology* **25**(2): 214–226.

Collins, WD, **Rasch, PJ**, **Eaton, BE**, **Khattatov, BV**, **Lamarque, JF**, **Zender, CS**. 2001. Simulating aerosols using a chemical transport model with assimilation of satellite aerosol retrievals: Methodology for INDOEX. *Journal of Geophysical Research: Atmospheres* **106**(D7): 7313–7336.

Cox, C, **Gallagher, M**, **Shupe, M**, **Persson, O**, **Solomon, A**, **Blomquist, B**, **Brooks, I**, **Costa, D**, **Gottas, D**, **Hutchings, J**, **Osborn, J**, **Morris, S**, **Preusser, A**, **Uttal, T**. 2021a. *10-meter (m) meteorological flux tower measurements (Level 1 Raw), Multidisciplinary drifting observatory for the study of arctic climate (MOSAiC), central Arctic, October 2019–September 2020*. Arctic Data Center. DOI: http://dx.doi.org/10.18739/A2VM42Z5F.

Cox, C, **Gallagher, M**, **Shupe, M**, **Persson, O**, **Solomon, A**, **Ayers, T**, **Costa, D**, **Hutchings, J**, **Leach, J**, **Morris, S**, **Osborn, J**, **Pezoa, S**, **Uttal, T**. 2021b. *Atmospheric surface flux station #30 measurements (Level 1 Raw), Multidisciplinary drifting observatory for the*

study of arctic climate (MOSAiC), central Arctic, October 2019–September 2020. Arctic Data Center. DOI: http://dx.doi.org/10.18739/A20C4SM1J.

Cox, C, **Gallagher, M**, **Shupe, M**, **Persson, O**, **Solomon, A**, **Ayers, T**, **Costa, D**, **Hutchings, J**, **Leach, J**, **Morris, S**, **Osborn, J**, **Pezoa, S**, **Uttal, T**. 2021c. *Atmospheric surface flux station #50 measurements (Level 1 Raw), Multidisciplinary drifting observatory for the study of arctic climate (MOSAiC), central Arctic, October 2019–September 2020*. Arctic Data Center. DOI: http://dx.doi.org/10.18739/A2445HD46.

Cox, C, **Gallagher, M**, **Shupe, M**, **Persson, O**, **Solomon, A**, **Ayers, T**, **Costa, D**, **Hutchings, J**, **Leach, J**, **Morris, S**, **Osborn, J**, **Pezoa, S**, **Uttal, T**. 2021d. *Atmospheric surface flux station #40 measurements (Level 1 Raw), Multidisciplinary drifting observatory for the study of arctic climate (MOSAiC), central Arctic, October 2019–September 2020*. Arctic Data Center. DOI: http://dx.doi.org/10.18739/A2CJ87M7G.

Curry, JA, **Schramm JL**, **Rossow, WB**, **Randall, D**. 1996. Overview of arctic cloud and radiation characteristics. *Journal of Climate* **9**: 1731–1764.

DeAngelis, AM, **Qu, X**, **Zelinka, MD**, **Hall, A**. 2015. An observational radiative constraint on hydrologic cycle intensification. *Nature* **528**(7581): 249–253.

Di Biagio, C, **Pelon, J**, **Blanchard, Y**, **Loyer, L**, **Hudson, SR**, **Walden, VP**, **Raut, JC**, **Kato, S**, **Mariage, V**, **Granskog, MA**. 2021. Toward a better surface radiation budget analysis over sea ice in the high Arctic Ocean: A comparative study between satellite, reanalysis, and local-scale observations. *Journal of Geophysical Research: Atmospheres* **126**(4). DOI: http://dx.doi.org/10.1e2020JD032555.

Dolinar, EK, **Dong, X**, **Xi, B**, **Jiang, JH**, **Su, H**. 2015. Evaluation of CMIP5 simulated clouds and TOA radiation budgets using NASA satellite observations. *Climate Dynamics* **44**(7): 2229–2247.

Duncan, BN, **Ott, LE**, **Abshire, JB**, **Brucker, L**, **Carroll, ML**, **Carton, J**, **Comiso, JC**, **Dinnat, EP**, **Forbes, BC**, **Gonsamo, A**, **Gregg, WW**. 2020. Space-based observations for understanding changes in the arctic-boreal zone. *Reviews of Geophysics* **58**(1). DOI: http://dx.doi.org/10.1e2019RG000652.

Fu, Q, **Lesins, G**, **Higgins, J**, **Charlock, T**, **Chylek, P**, **Michalsky, J**. 1998. Broadband water vapor absorption of solar radiation tested using ARM data. *Geophysical Research Letters* **25**(8): 1169–1172.

Fu, Q, **Liou, KN**. 1993. Parameterization of the radiative properties of cirrus clouds. *Journal of Atmospheric Sciences* **50**(13): 2008–2025.

Grenfell, TC, **Perovich, DK**. 2008. Incident spectral irradiance in the Arctic Basin during the summer and fall. *Journal of Geophysical Research: Atmospheres* **113**: D12117. DOI: http://dx.doi.org/10.1029/2007JD009418.

Hakuba, MZ, **Folini, D**, **Wild, M**. 2016. On the zonal near-constancy of fractional solar absorption in the atmosphere. *Journal of Climate* **29**(9): 3423–3440.

Hess, M, **Koepke, P**, **Schult, I**. 1998. Optical properties of aerosols and clouds: The software package OPAC. *Bulletin of the American meteorological society* **79**(5): 831–844.

Holland, MM, **Bitz, CM**. 2003. Polar amplification of climate change in coupled models. *Climate Dynamics* **21**(3–4): 221–232.

Huang, Y, **Dong, X**, **Bailey, DA**, **Holland, MM**, **Xi, B**, **DuVivier, AK**, **Kay, JE**, **Landrum, LL**, **Deng, Y**. 2019. Thicker clouds and accelerated Arctic sea ice decline: The atmosphere-sea ice interactions in spring. *Geophysical Research Letters* **46**(12): 6980–6989.

Huang, Y, **Dong, X**, **Xi, B**, **Dolinar, EK**, **Stanfield, RE**. 2017a. The footprints of 16 year trends of Arctic springtime cloud and radiation properties on September sea ice retreat. *Journal of Geophysical Research: Atmospheres* **122**(4): 2179–2193.

Huang, Y, **Dong, X**, **Xi, B**, **Dolinar, EK**, **Stanfield, RE**, **Qiu, S**. 2017b. Quantifying the uncertainties of reanalyzed Arctic cloud and radiation properties using satellite surface observations. *Journal of Climate* **30**(19): 8007–8029.

Jin, Z, **Charlock, TP**, **Smith, WL**, **Jr, Rutledge, K**. 2004. A parameterization of ocean surface albedo. *Geophysical Research Letters* **31**(22): L22301. DOI: http://dx.doi.org/10.1029/2004GL021180

Kato, S, **Ackerman, TP**, **Mather, JH**, **Clothiaux, EE**. 1999. The k-distribution method and correlated-k approximation for a shortwave radiative transfer model. *Journal of Quantitative Spectroscopy and Radiative Transfer* **62**(1): 109–121.

Kato, S, **Rose, FG**, **Charlock, TP**. 2005. Computation of domain-averaged irradiance using satellite-derived cloud properties. *Journal of Atmospheric and Oceanic Technology* **22**(2): 146–164.

Kato, S, **Rose, FG**, **Rutan, DA**, **Thorsen, TJ**, **Loeb, NG**, **Doelling, DR**, **Huang, X**, **Smith, WL**, **Su, W**, **Ham, SH**. 2018. Surface irradiances of edition 4.0 Clouds and the Earth's Radiant Energy System (CERES) Energy Balanced and Filled (EBAF) data product. *Journal of Climate* **31**(11): 4501–4527.

Kato, S, **Smith, GL**, **Barker, HW**. 2001. Gamma-weighted discrete ordinate two-stream approximation for computation of domain-averaged solar irradiance. *Journal of the Atmospheric Sciences* **58**(24): 3797–3803.

Kratz, DP, **Rose, FG**. 1999. Accounting for molecular absorption within the spectral range of the CERES window channel. *Journal of Quantitative Spectroscopy and Radiative Transfer* **61**(1): 83–95.

Lee, S, **Gong, T**, **Feldstein, SB**, **Screen, JA**, **Simmonds, I**. 2017. Revisiting the cause of the 1989–2009 Arctic surface warming using the surface energy budget: Downward infrared radiation dominates the surface fluxes. *Geophysical Research Letters* **44**(20): 10–654.

Lesins, G, **Duck, TJ**, **Drummond, JR**. 2012. Surface energy balance framework for Arctic amplification of climate change. *Journal of Climate* **25**(23): 8277–8288.

Light, B, **Smith, MS**, **Perovich, DK**, **Webster, MA**, **Holland, M**, **Linhardt, F**, **Raphael, IA**, **Clemens-Sewall, D**,

MacFarlane, A, **Anhaus, P**, **Bailey D**. 2021. Arctic sea ice albedo: Spectral composition, spatial heterogeneity, and temporal evolution observed during the MOSAiC drift. *Elementa: Science of the Anthropocene*, in press.

Marty, C, **Philipona, R**, **Delamere, J**, **Dutton, EG**, **Michalsky, J**, **Stamnes, K**, **Storvold, R**, **Stoffel, T**, **Clough, SA**, **Mlawer, EJ**. 2003. Downward longwave irradiance uncertainty under arctic atmospheres: Measurements and modeling. *Journal of Geophysical Research: Atmospheres* **108**(D12): 1–12.

Nixdorf, U, **Dethloff, K**, **Rex, M**, **Shupe, M**, **Sommerfeld, A**, **Perovich, DK**, **Nicolaus, M**, **Heuze, C**, **Rabe, B**, **Loose, B**, **Damm, E**, **Gradinger, R**, **Fong, A**, **Maslowski, W**, **Rinke, A**, **Kwok, R**, **Spreen, G**, **Wendisch, m**, **Herber, A**, **Hirsekorn, M**, **Mohaupt, V**, **Frickenhaus, S**, **Immerz, A**, **Weiss-Tuider, K**, **Koenig, B**, **Mengedoht, D**, **Regnery, J**, **Gerchow, P**, **Ransby, D**, **Krumpen, T**, **Morgenstern, A**, **Haas, C**, **Kanzow, T**, **Rack, F**, **Saitzev, V**, **Sokolov, V**, **Makarov, A**, **Schwarze, S**, **Wunderlick, T**, **Wurr, K**, **Boetius, A**. 2021. MOSAiC extended acknowledgement. *Zenodo*. DOI: http://dx.doi.org/10.5281/zenodo.5541624.

Persson, POG. 2012. Onset and end of the summer melt season over sea ice: Thermal structure and surface energy perspective from SHEBA. *Climate Dynamics* **39**(6): 1349–1371.

Persson, POG, **Fairall, CW**, **Andreas, EL**, **Guest, PS**, **Perovich, DK**. 2002. Measurements near the Atmospheric Surface Flux Group tower at SHEBA: Near-surface conditions and surface energy budget. *Journal of Geophysical Research: Oceans* **107**(C10): SHE-21.

Remer, LA, **Kaufman, YJ**, **Tanré, D**, **Mattoo, S**, **Chu, DA**, **Martins, JV**, **Li, RR**, **Ichoku, C**, **Levy, RC**, **Kleidman, RG**, **Eck, TF**. 2005. The MODIS aerosol algorithm, products, and validation. *Journal of Atmospheric Sciences*, **62**(4): 947–973.

Riihelä, A, Key, JR, **Meirink, JF**, **Kuipers Munneke, P**, **Palo, T**, **Karlsson, KG**. 2017. An intercomparison and validation of satellite-based surface radiative energy flux estimates over the Arctic. *Journal of Geophysical Research: Atmospheres* **122**(9): 4829–4848.

Riihimaki, L. 2021. *Radiation instruments on Ice (ICERADRIIHIMAKI)*. Atmospheric Radiation Measurement (ARM) User Facility. DOI: http://dx.doi.org/10.5439/1608608.

Rose, FG, **Charlock, T**, **Fu, Q**, **Kato, S**, **Rutan, D**, **Jin, J**. 2006. CERES proto-edition 3 radiative transfer: Model tests and radiative closure over surface validation sites. 12th Conf. on Atmospheric Radiation, Madison, WI, Amer. Meteor. Soc., P2.4. DOI: https://ams.confex.com/ams/Madison2006/techprogram/paper_112358.htm.

Rose, FG, **Rutan, DA**, **Charlock, T**, **Smith, GL**, **Kato, S**. 2013. An algorithm for the constraining of radiative transfer calculations to CERES-observed broadband top-of-atmosphere irradiance. *Journal of Atmospheric and Oceanic Technology* **30**(6): 1091–1106.

Rutan, D, **Rose, F**, **Roman, M**, **Manalo-Smith, N**, **Schaaf, C**, **Charlock, T**. 2009. Development and assessment of broadband surface albedo from clouds and the earth's radiant energy system clouds and radiation swath data product. *Journal of Geophysical Research: Atmospheres* **114**(D08125): 1–19.

Rutan, DA, **Kato, S**, **Doelling, DR**, **Rose, FG**, **Nguyen, LT**, **Caldwell, TE**, **Loeb, NG**. 2015. CERES synoptic product: Methodology and validation of surface radiant flux. *Journal of Atmospheric and Oceanic Technology* **32**(6): 1121–1143.

Shupe, MD, **Intrieri, JM**. 2004. Cloud radiative forcing of the Arctic surface: The influence of cloud properties, surface albedo, and solar zenith angle. *Journal of Climate* **17**: 616–628.

Shupe, MD, **Rex, M**, **Blomquist, B**, **Persson, POG**, **Schmale, J**, **Uttal, T**, **Althausen, D**, **Angot, H**, **Archer, S**, **Bariteau, L**, **Beck, I**, **Bilberry, J**, **Bussi, S**, **Buck, C**, **Boyer, M**, **Brasseur, Z**, **Brooks, IM**, **Calmer, R**, **Cassano, J**, **Castro, V**, **Chu, D**, **Costa, D**, **Cox, CJ**, **Creamean, J**, **Crewell, S**, **Dahlke, S**, **Damm, E**, de Boer, G, **Deckelmann, H**, **Dethloff, K**, **Dütsch, M**, **Ebell, K**, **Ehrlich, A**, **Ellis, J**, **Engelmann, R**, **Fong, AA**, **Frey, MM**, **Gallagher, MR**, **Ganzeveld, L**, **Gradinger, R**, **Graeser, J**, **Greenamyer, V**, **Griesche, H**, **Griffiths, S**, **Hamilton, J**, **Heinemann, G**, **Helmig, D**, **Herber, A**, **Heuzé, C**, **Hofer, J**, **Houchens, T**, **Howard, D**, **Inoue, J**, **Jacobi, H-W**, **Jaiser, R**, **Jokinen, T**, **Jourdan, O**, **Jozef, G**, **King, W**, **Kirchgaessner, A**, **Klingebiel, M**, **Krassovski, M**, **Krumpen, T**, **Lampert, A**, **Landing, W**, **Laurila, T**, **Lawrence, D**, **Loose, B**, **Lonardi, M**, **Lüpkes, C**, **Maahn, M**, **Macke, A**, **Maslowski, W**, **Marsay, C**, **Maturilli, M**, **Mech, M**, **Morris, S**, **Moser, M**, **Nicolaus, M**, **Ortega, P**, **Osborn, J**, **Pätzold, F**, **Perovich, DK**, **Petäjä, T**, **Pilz, C**, **Pirazzini, R**, **Posman, K**, **Powers, H**, **Pratt, KA**, **Preußer, A**, **Quéléver, L**, **Radenz, M**, **Rabe, B**, **Rinke, A**, **Sachs, T**, **Schulz, A**, **Siebert, H**, **Silva, T**, **Solomon, A**, **Sommerfeld, A**, **Spreen, G**, **Stephens, M**, **Stohl, A**, **Svensson, G**, **Uin, J**, **Viegas, J**, **Voigt, C**, **von der Gathen, P**, **Wehner, B**, **Welker, JM**, **Wendisch, M**, **Werner, M**, **Xie, Z**, **Yue, F**. 2021. Overview of the MOSAiC expedition: Atmosphere. *Elementa: Science of the Anthropocene* **10**(1). DOI: https://dx.doi.org/10.1525/elementa.2021.00060.

Shupe, MD, **Rex, M**, **Dethloff, K**, **Damm, E**, **Fong, AA**, **Gradinger, R**, **Heuze, C**, **Loose, B**, **Makarov, A**, **Maslowski, W**, **Nicolaus, M**. 2020. The MOSAiC expedition: A year drifting with the Arctic Sea ice. *Arctic Report Card*. DOI: https://dx.doi.org/10.25923/9g3v-xh92.

Smith, M, **Light, B**, **Perovich, D**, **Webster, M**, **Anhaus, P**, **Clemens-Sewall, D**, **Linhardt, F**, **Macfarlane, A**, **Raphael, I**, **Bozzato, D**, **Brasseur, Z**, **Dadic, R**, **Fons, S**, **Immerz, A**, **Hannula, H**, **Hutchings, J**, **Pätzold, F**, **Regnery, J**, **Pirazzini, R**, **Tavri, A**. 2021a. *Spectral albedo measurements of the sea ice surface during the Multidisciplinary drifting Observatory for the Study of Arctic Climate (MOSAiC)*

campaign in the Central Arctic Ocean, April–September 2020. Arctic Data Center. DOI: https://dx.doi.org/10.18739/A2FT8DK8Z.

Smith, M, **Light, B**, **Perovich, D**, **Webster, M**, **Anhaus, P**, **Clemens-Sewall, D**, **Linhardt, F**, **Macfarlane, A**, **Raphael, I**, **Bozzato, D**, **Brasseur, Z**, **Dadic, R**, **Fons, S**, **Immerz, A**, **Hannula, H**, **Hutchings, J**, **Pätzold, F**, **Regnery, J**, **Pirazzini, R**, **Tavri, A**. 2021b. *Broadband albedo measurements of the sea ice surface during the Multidisciplinary drifting observatory for the study of arctic climate (MOSAiC) campaign in the Central Arctic Ocean, April–September 2020*. Arctic Data Center. DOI: https://dx.doi.org/10.18739/A2KK94D36.

Smith, WL, Jr., Hansen, C, Bucholtz, A, Anderson, BE, Beckley, M, Corbett, JG, Cullather, RI, Hines, KM, Hofton, M, Kato, S, Lubin, D, Moore, RH, Segal Rosenhaimer, M, Redemann, J, Schmidt, S, Scott, R, Song, S, Barrick, JD, Bryan Blair, J, Bromwich, DH, Brooks, C, Chen, G, Cornejo, H, Corr, CA, Ham, S-H, Scott Kittelman, A, Knappmiller, S, LeBlanc, S, Loeb, NG, Miller, C, Nguyen, L, Palikonda, R, Rabine, D, Reid, EA, Richter-Menge, JA, Pilewskie, P, Shinozuka, Y, Spangenberg, D, Stackhouse, P, Taylor, P, Lee Thornhill, K, van Gilst, D, Winstead, E. 2017. Arctic Radiation-IceBridge Sea and Ice Experiment (ARISE): The Arctic Radiant Energy System during the critical seasonal ice transition. *Bulletin of the American Meteorological Society* **98**(7): 1399–1426. DOI: https://dx.doi.org/10.1175/BAMS-D-14-00277.1.

Su, W, **Corbett, J**, **Eitzen, Z**, **Liang, L**. 2015. Next-generation angular distribution models for top-of-atmosphere radiative flux calculation from CERES instruments: Validation. *Atmospheric Measurement Techniques* **8**(8): 3297–3313.

Taylor, PC, **Boeke, RC**, **Boisvert, LN**, **Feldl, N**, **Henry, M**, **Huang, Y**, **Langen, PL**, **Liu, W**, **Pithan, F**, **Sejas, S**, **Tan, I**. 2021. Process drivers, inter-model spread, and the path forward: A review of amplified Arctic warming. *Frontiers in Earth Science* **9**. DOI: https://dx.doi.org/10.3389/feart.2021.758361.

Tegen, I, **Lacis, AA**. 1996. Modeling of particle size distribution and its influence on the radiative properties of mineral dust aerosol. *Journal of Geophysical Research: Atmospheres* **101**(D14): 19237–19244.

Toon, OB, **McKay, CP**, **Ackerman, TP**, **Santhanam, K**. 1989. Rapid calculation of radiative heating rates and photodissociation rates in inhomogeneous multiple scattering atmospheres. *Journal of Geophysical Research: Atmospheres* **94**(D13): 16287–16301.

Walsh, JE, **Chapman, WL**, **Portis, DH**. 2009. Arctic cloud fraction and radiative fluxes in atmospheric reanalyses. *Journal of Climate* **22**(9): 2316–2334.

Wendler, G, **Moore, B**, **Hartmann, B**, **Stuefer, M**, **Flint, R**. 2004. Effects of multiple reflection and albedo on the net radiation in the pack ice zones of Antarctica. *Journal of Geophysical Research: Atmospheres* **109**(D09113): 1–8.

Wilber, AC, **Kratz, DP**, **Gupta, SK**. 1999. *Surface emissivity maps for use in satellite retrievals of longwave radiation*. Hampton, VA: National Aeronautics and Space Administration. NASA Tech. Publ. NASA/TP-1999-209362, 35 p.

Wild, M. 2020. The global energy balance as represented in CMIP6 climate models. *Climate Dynamics* **55**: 553–577.

Wild, M, **Folini, D**, **Hakuba, MZ**, **Schär, C**, **Seneviratne, SI**, **Kato, S**, **Rutan, D**, **Ammann, C**, **Wood, EF**, **König-Langlo, G**. 2015. The energy balance over land and oceans: An assessment based on direct observations and CMIP5 climate models. *Climate Dynamics* **44**(11–12): 3393–3429.

Yang, S-K, **Zhou, S**, **Miller, AJ**. 1998. SMOBA: A 3-dimensional daily ozone analysis using SBUV/2 and TOVS measurements. DOI: http://www.cpc.ncep.noaa.gov/products/stratosphere/SMOBA/smoba_doc.shtml. Accessed 6 January 2015.

Yost, CR, **Minnis, P**, **Sun-Mack, S**, **Chen, Y**, **Smith, WL**. 2020. CERES MODIS cloud product retrievals for edition 4—Part II: Comparisons to CloudSat and CALIPSO. *IEEE Transactions on Geoscience and Remote Sensing* **59**(5): 3695–3724.

How to cite this article: Huang, Y, Taylor, PC, Rose, FG, Rutan, DA, Shupe, MD, Webster, MA, Smith, MM. 2022. Toward a more realistic representation of surface albedo in NASA CERES-derived surface radiative fluxes: A comparison with the MOSAiC field campaign. *Elementa: Science of the Anthropocene* 10(1). DOI: https://doi.org/10.1525/elementa.2022.00013

Domain Editor-in-Chief: Detlev Helmig, Boulder AIR LLC, Boulder, CO, USA

Associate Editor: Joël Savarino, Laboratoire de Glaciologie et Géophysique de l'Environnement, CNRS/Grenoble University, Saint-Martin d'Hères, France

Knowledge Domain: Atmospheric Science

Part of an Elementa Special Feature: The Multidisciplinary Drifting Observatory for the Study of Arctic Climate (MOSAiC)

Published: June 1, 2022 **Accepted:** April 28, 2022 **Submitted:** January 21, 2022

ELEMENTA Science of the Anthropocene

Elem Sci Anth is a peer-reviewed open access journal published by University of California Press.

OPEN ACCESS